Molecular Pharmacology Fast Forward. Published on October 11, 2007 as DOI: 10.1124/mol.107.039180

MOL #39180

Subcellular Trafficking, Pentameric Assembly and Subunit Stoichiometry of Neuronal Nicotinic ACh Receptors Containing Fluorescently-Labeled α6 and β3 Subunits.

Ryan M. Drenan, Raad Nashmi, Princess Imoukhuede, Herwig Just, Sheri McKinney, Henry A. Lester

R.M.D., R.N., P.I., H.J., S.M., H.A.L.: Division of Biology, California Institute of Technology, Pasadena, CA 91125

Molecular Pharmacology Fast Forward. Published on October 11, 2007 as DOI: 10.1124/mol.107.039180
This article has not been copyedited and formatted. The final version may differ from this version.

Running Title Page

Running Title: Fluorescent α6* and β3* Nicotinic ACh Receptors

Corresponding Author:

Henry A. Lester

California Institute of Technology

Division of Biology, M/C 156-29

1200 E. California Blvd.

Pasadena, CA 91125

Tel: 626-395-4946

Fax: 626-564-8709

E-mail: lester@caltech.edu

Text Pages: 58

Tables: 1

Figures: 11

References: 40

Words: Abstract: 238

Introduction: 744

Discussion: 1486

Nonstandard Abbreviations: FRET, Förster resonance energy transfer; TIRF, total internal reflection fluorescence; VTA, ventral tegmental area; CSF, cerebrospinal fluid; HEK293, human embryonic kidney 293; PKA, protein kinase A;

Molecular Pharmacology Fast Forward. Published on October 11, 2007 as DOI: 10.1124/mol.107.039180
This article has not been copyedited and formatted. The final version may differ from this version.

Abstract

Neuronal nicotinic ACh receptors are ligand-gated, cation-selective ion channels. Nicotinic receptors containing α4, α6, β2, and β3 subunits are expressed in midbrain dopaminergic neurons and are implicated in the response to smoked nicotine. Here we have studied the cell biological and biophysical properties of receptors containing α6 and β3 subunits by utilizing fluorescent proteins fused within the M3-M4 intracellular loop. Receptors containing fluorescently-tagged β3 subunits were fully functional compared to receptors with untagged β3 subunits. We find that β3 and α6-containing receptors are highly expressed in neurons, and co-localize with co-expressed, fluorescent α4 and β2 subunits in neuronal soma and dendrites. Förster resonance energy transfer (FRET) reveals efficient, specific assembly of β3 and α6 into nicotinic receptor pentamers of various subunit compositions. Using FRET, we demonstrate directly that only a single β3 subunit is incorporated into nAChRs containing this subunit, whereas multiple subunit stoichiometries exist for α4 and α6-containing receptors. Finally, we demonstrate that nicotinic ACh receptors are localized in distinct microdomains at or near the plasma membrane using total internal reflection fluorescence (TIRF) microscopy. We suggest that neurons contain large, intracellular pools of assembled, functional nicotinic receptors, which may provide them with the ability to rapidly up-regulate nicotinic responses to endogenous ligands such as ACh, or to exogenous agents such as nicotine. Further, this report is the first to directly measure nAChR subunit stoichiometry using FRET and plasma membrane localization of α6 and β3-containing receptors using TIRF.

Molecular Pharmacology Fast Forward. Published on October 11, 2007 as DOI: 10.1124/mol.107.039180
This article has not been copyedited and formatted. The final version may differ from this version.

Introduction

α6 nicotinic ACh receptor subunits are expressed in several catecholaminergic nuclei in the central nervous system, including retinal ganglion cells (Gotti et al., 2005b), locus coeruleus (Lena et al., 1999), and dopaminergic neurons located in the substantia nigra (SN) and ventral tegmental area (VTA) (Champtiaux et al., 2003; Whiteaker et al., 2000; Zoli et al., 2002). Ligand-binding studies using the α6-specific probe α-conotoxin MII suggest that many α6* (* = other subunits may be present in the receptor) receptors are located on presynaptic terminals in the superior colliculus and striatum (Whiteaker et al., 2000). Indeed, this binding activity disappears in the brains of α6 knockout mice (Champtiaux et al., 2002). This strikingly specific expression pattern could indicate a unique function for α6* receptors, and α6* receptors are candidate drug targets for diseases or disorders such as Parkinson's disease or nicotine addiction (Quik and McIntosh, 2006).

Functional, voltage-clamped α6-dependent responses are elusive in heterologous expression systems such as *Xenopus* oocytes (Broadbent et al., 2006; Kuryatov et al., 2000), but native α6* receptors are readily studied using synaptosome preparations from brain tissue (Champtiaux et al., 2003; Gotti et al., 2005a; Grady et al., 2002; Whiteaker et al., 2000). Indeed, α-conotoxin MII-sensitive receptors are pharmacologically and stoichiometrically distinct from α-conotoxin MII-resistant receptors in mediating [^{3}H]-dopamine release from striatal synaptosomes (Grady et al., 2002; Salminen et al., 2007). Recent studies utilizing α4 and β3 knockout mice demonstrate the existence of functional α6β2, α6β2β3, α6α4β2, and α6α4β2β3 receptors (Salminen et al., 2007). Importantly, native α6α4β2β3 receptors have the highest affinity (EC_{50} = 0.23 $\pm$ 0.08 μM) for nicotine

Molecular Pharmacology Fast Forward. Published on October 11, 2007 as DOI: 10.1124/mol.107.039180
This article has not been copyedited and formatted. The final version may differ from this version.

of any nicotinic receptor reported to date. Because nicotine is likely to be present at concentrations $\leq$ 0.5 μM in the CSF of smokers (Rowell, 2002), only those receptors with the highest affinity for nicotine, including some α4* and α6* receptors, are likely to be important in nicotine addiction. Although previous studies offer major conceptual advances in our understanding of α6* receptors in the brain, there is a lack of information regarding the subcellular localization and biophysical properties of α6 subunits.

β3 subunits are expressed in most of the same locations as α6, including midbrain dopaminergic neurons projecting to the striatum (Zoli et al., 2002). β3 knockout mice demonstrate that β3 subunits are important for the biogenesis of α6* receptors in the brain (Cui et al., 2003; Gotti et al., 2005a). This is corroborated by studies in *Xenopus* oocytes and tissue culture cells (Kuryatov et al., 2000). β3 also increases α6-specific binding activity in HEK293 cells (Tumkosit et al., 2006). Uncertainty exists however, as others have reported that β3 incorporation into nAChRs acts as a dominant negative (Boorman et al., 2003; Broadbent et al., 2006), suppressing ACh-evoked responses by an incompletely understood gating mechanism. This effect occurred apparently without significantly altering the surface expression of nAChRs. What is clear is that β3 acts more like a muscle β subunit than a "typical" neuronal β subunit; it does not participate in forming the α:non-α interface that comprises the neuronal ligand binding site, and other β subunits, either β2 or β4, must be present to form functional nicotinic receptors (Broadbent et al., 2006). This presents a problem both for basic and therapeutic-oriented research on β3* receptors, as there are no pharmacological ligands that can visually or functionally isolate β3-specific actions in cell culture systems or intact brain tissue.

Molecular Pharmacology Fast Forward. Published on October 11, 2007 as DOI: 10.1124/mol.107.039180
This article has not been copyedited and formatted. The final version may differ from this version.

Given the precise localization and unique functional properties of β3* receptors, potential for therapeutic intervention that would be afforded by β3-specific probes, and involvement in nicotine addiction (Bierut et al., 2007), it is important to develop and exploit tools to study β3.

We have sought to compare characteristics of α6 and β3 with the better-understood α4 and β2 subunits. We previously generated fluorescently labeled α4 and β2 subunits and employed these subunits to study assembly, trafficking, and nicotine-dependent upregulation of α4β2 receptors (Nashmi et al., 2003). We have now fluorescently-labeled α6 and β3 subunits by inserting a yellow fluorescent protein (YFP) or cyan fluorescent protein (CFP) in the M3-M4 intracellular loop. With this approach, one can optically monitor functional nicotinic ACh receptors containing these subunits in live cells and in real time. We measured: 1) functional responses using two-electrode voltage clamp and patch clamp electrophysiology, 2) subcellular distribution and co-localization in neurons using confocal microscopy and spectral imaging, 3) receptor assembly and subunit stoichiometry using Förster resonance energy transfer (FRET), and 4) plasma membrane localization and distribution patterns using total internal reflection fluorescence (TIRF) microscopy.

Molecular Pharmacology Fast Forward. Published on October 11, 2007 as DOI: 10.1124/mol.107.039180
This article has not been copyedited and formatted. The final version may differ from this version.

Materials and Methods

Reagents - Unless otherwise noted, all chemicals were from Sigma (St. Louis, MO). DNA oligonucleotides for PCR and site-directed mutagenesis were synthesized by Integrated DNA Technologies (Coralville, IA). Restriction enzymes for molecular biology were purchased from Roche Diagnostics (Indianapolis, IN) or New England Biolabs (Ipswich, MA). 35 mm glass-bottom dishes coated with L-polylysine were purchased from MatTek (Ashland, MA).

Cell Culture and Transfection - N2a cells (ATCC) were maintained in Dulbecco's modified Eagle's medium (high glucose with 4 mM L-glutamine, Invitrogen; Carlsbad, CA)/Optimem (Invitrogen) mixed at a ratio of 1:1 and supplemented with 10% fetal bovine serum (Invitrogen), penicillin (Mediatech; Herndon, VA) and streptomycin (Invitrogen). N2a cells were transfected in DMEM without serum or antibiotics. Transfection was carried out using Lipofectamine/PLUS (Invitrogen) according to the manufacturer's instructions and with the following modifications. For a 35 mm dish, 1-2 µg of total plasmid DNA was mixed with 100 µl DMEM and 6 µl PLUS reagent. DMEM/DNA was combined with a mixture of 100 µl DMEM and 4 µl Lipofectamine reagent. Rat hippocampal neurons were dissociated and plated on glass-bottom imaging dishes as described (Slimko et al., 2002). For primary neuron transfection, Lipofectamine 2000 (Invitrogen) was used in conjunction with Nupherin (Biomol Research Laboratories; Plymouth Meeting, PA) as described below. Briefly, a total of 1 µg of DNA was incubated with 20 µg of Nupherin in 400 µl of Neurobasal medium without phenol red (Invitrogen) while 10 µl of Lipofectamine 2000 was mixed in 400 µl of Neurobasal

(Invitrogen). After 15 min the two solutions were combined and incubated for 45 min. Neuronal cultures in 35 mm glass-bottom culture dishes were incubated in the resulting 800 µl mixture for 120 min, followed by removal of transfection media and re-feeding of the original, pre-transfection culture media.

Plasmids and Molecular Biology - Mouse α4 and β2 nAChR cDNAs in pCI-neo, both untagged and modified with YFP or CFP fluorescent tags, have been previously described (Nashmi et al., 2003). Mouse α3 and β3 nAChR cDNAs in pCDNA3.1 were a generous gift of Jerry Stitzel (Institute for Behavioral Genetics; University of Colorado). A full-length mouse α6 I.M.A.G.E. cDNA (ID# 4501558) was obtained from Open Biosystems (Huntsville, AL). A modified α6 cDNA was constructed that 1) lacked the 5' and 3' UTRs and 2) contained a Kozak sequence (GCC ACC) prior to the ATG start codon to facilitate efficient translation initiation. Rat β4 cloned into pAMV was provided by Cesar Labarca (California Institute of Technology). pEYFP-N1 and pECFP-N1 (Clontech; Mountain View, CA) were used to construct fluorescent nAChR cDNAs. mGAT1 labeled with CFP was provided by Fraser Moss (California Institute of Technology). YFP-Syntaxin was provided by Wolfhard Almers (Vollum Institute; Oregon Health & Science University). CFP-tau was provided by George Bloom (University of Virginia). A QuikChange (Stratagene) kit was used to construct β3 (WT or XFP-modified) cDNAs containing a V13'S point mutation.

To design fluorescently-labeled α6 and β3 subunits, we chose to insert the XFP moiety in the M3-M4 loop each subunit. We have previously found that this region is appropriate for insertion in nAChR α4 and β2 subunits (Nashmi et al., 2003), the nAChR

Molecular Pharmacology Fast Forward. Published on October 11, 2007 as DOI: 10.1124/mol.107.039180
This article has not been copyedited and formatted. The final version may differ from this version.

γ subunit (data not shown), and GluCl α and β subunits (Slimko et al., 2002). Similar to our previous studies, we inserted the XFP moiety in the M3-M4 loop at positions that avoided the conserved amphipathic α-helix as well as putative cell sorting motifs and phosphorylation sites (Fig. 1A and B). To construct nAChRs with XFP inserted into the M3-M4 loop, a two-step PCR protocol was used. First, YFP or CFP was amplified with PCR using oligos (sequences available upon request) designed to engineer 5' and 3' overhangs of 15 bp which was identical to the site where XFP was to be inserted, in frame, into the nAChR M3-M4 loop. A Gly-Ala-Gly flexible linker was engineered between the nAChR sequence and the sequence for YFP/CFP at both the 5' and 3' ends. In the second PCR step, 100 ng of the first PCR reaction was used as a primer pair in a modified QuikChange reaction using Pfu Ultra II (Stratagene; Cedar Creek, TX) polymerase and the appropriate nAChR cDNA as a template. All DNA constructs were confirmed with sequencing and, in some cases, restriction mapping.

cRNA for injection and expression in *Xenopus laevis* oocytes was prepared using a T7 or SP6 in vitro transcription kit (mMessage mMachine, Ambion; Foster City, CA) according to the manufacturer's instructions. RNA yield was quantified with absorbance at 260 nm. RNA quality was assessed by observing absorbance profiles across a range of wavelengths between 220 nm and 320 nm. Spectrophotometric analysis was performed using a ND-1000 spectrophotometer (NanoDrop; Wilmington, DE).

Confocal Microscopy - N2a cells were plated on 35 mm glass-bottom dishes, transfected with nAChR cDNAs, and imaged live 24-48 hours after transfection. *Xenopus* oocytes were imaged 3 days after RNA injection. Oocytes were placed in an imaging chamber

and allowed to settle for 20 min prior to imaging. To eliminate autofluorescence, growth medium was replaced with an extracellular solution containing the following components (in mM): 150 NaCl, 4 KCl, 2 $CaCl_2$, 2 $MgCl_2$, 10 HEPES, and 10 D-glucose, pH 7.4. Cells were imaged with a Nikon (Nikon Instruments; Melville, NY) C1 laser-scanning confocal microscope system equipped with spectral imaging capabilities and a Prior (Rockland, MA) remote-focus device. For oocytes, a Nikon Plan Apo 20X 0.75 NA air objective was used, whereas a Nikon Plan Apo 60X 1.40 NA oil objective was used for mammalian tissue culture cells. Pinhole diameter was 30-60 μm, and cells were imaged at 12-bit intensity resolution over 512 X 512 pixels at a pixel dwell time of 4-6 μs. CFP was excited using a 439.5 nm modulated diode laser, and YFP was excited with an argon laser at 514.5 nm. In most cases, imaging was carried out using the Nikon C1si DEES grating and spectral detector with 32 parallel photomultiplier tubes (PMT). This allowed us to collect spectral images (lambda stacks). In such images, each pixel of the X-Y image contains a list of emission intensity values across a range of wavelengths. We collected light between 450 nm and 600 nm at a bandwidth of 5 nm. The 515 nm channel was intentionally blocked while we used the 514.5 nm laser for YFP bleaching. Because the emission profile of YFP and CFP significantly overlap, we used the Nikon EZC1 linear unmixing algorithm to reconstruct YFP and CFP images. Experimental spectral images with both YFP and CFP-labeled nAChR subunits were unmixed using reference spectra from images with only YFP or CFP-labeled nAChR subunits. For each pixel of a spectral image, intensity of YFP and CFP was determined from fluorescence intensity values at the peak emission wavelength derived from the reference spectra.

Molecular Pharmacology Fast Forward. Published on October 11, 2007 as DOI: 10.1124/mol.107.039180
This article has not been copyedited and formatted. The final version may differ from this version.

Spectral FRET Analysis - To examine Förster resonance energy transfer (FRET) between various nAChR subunits, the acceptor photobleaching method (Nashmi et al., 2003) was employed by using a modified fluorescence recovery after photobleaching (FRAP) macro built into the Nikon EZC1 imaging software. In this method, FRET was detected by recording CFP dequenching during incremental photodestruction of YFP. A spectral image was acquired once before YFP bleaching, and at six time points every ten seconds during YFP bleaching at 514.5 nm. Laser power during bleaching varied from cell to cell, but was between 25-50%. One bleach scan per cycle was used. This bleaching protocol was optimized to achieve 70-80% photodestruction of YFP while still enabling us to record incremental increases in CFP emission at each time point. In the confocal microscope, nAChRs labeled with XFP usually exhibit a uniform, intracellular distribution, regardless of the subunit being examined. This is consistent with our previous observations (Nashmi et al., 2003). To measure FRET, spectral images were unmixed into their CFP and YFP components as described above. We found little or no difference in FRET for various cellular structures or organelles in N2a cells, and we measured CFP and YFP mean intensity throughout the entire cell by selecting the cell perimeter as the boundary of a region of interest in Nikon's EZC1 software. CFP and YFP components were saved in Excel format, and fluorescence intensities were normalized to the pre-bleach time point (100%). FRET efficiency (E) was calculated as:

$$E = 1 - (I_{DA}/I_D)$$

I_{DA} represents the normalized fluorescence intensity of CFP (100%) in the presence of both donor (CFP) and acceptor (YFP). I_D represents the normalized fluorescence intensity of CFP in the presence of donor only (complete photodestruction of YFP). The I_D value

was extrapolated from a scatter plot of the fractional increase of CFP versus the fractional decrease of YFP. FRET efficiency (*E*) values were averaged from several cells per condition (see Table 1 for *n* values). Data are reported as mean ± SEM.

Total Internal Reflection Fluorescence (TIRF) Microscopy – N2a cells cultured in glass-bottom, polyethylenimine-coated imaging dishes were transfected with cDNA mixtures as described above. Cells, superfused with the same imaging solution used for confocal microscopy, were imaged 18-24 hours after transfection to minimize overexpression artifacts. TIRF images were obtained with an inverted microscope (Olympus IX71, Olympus America, Inc.; Center Valley, PA) equipped with a 488 nm air-cooled argon laser (Melles Griot; Carlsbad, CA, P/N IMA101040ALS). Laser output was controlled with a UNIBLITZ shutter system and drive unit (Vincent Associates; Rochester, NY, P/N VMM-D1) equipped with a Mitutoyo (Mitutoyo America; City of Industry, CA) micrometer to control TIRF evanescent field illumination. TIRF imaging was carried out with an Olympus PlanApo 100X 1.45NA oil objective, and images were captured with a 16 bit resolution Photometrics Cascade CCD camera (Photometrics; Tucson, AZ) controlled by Slidebook 4.0 imaging software (Intelligent Imaging Innovations; Santa Monica, CA).

Two-Electrode Voltage Clamp Electrophysiology - Stage V-VI *Xenopus* oocytes were isolated as described (Quick and Lester, 1994). Stock RNAs were diluted into DEPC-treated water and injected one day after isolation. RNA was injected in a final volume of 50 nl per oocyte using a digital microdispenser (Drummond; Broomall, PA). After

injection, oocytes were incubated in ND-96 solution (in mM: 96 NaCl, 2 KCl, 1 $CaCl_2$, 1 $MgCl_2$, 5 Hepes/NaOH, pH 7.6) supplemented with Gentamycin (50 µg/ml) and sodium pyruvate (2.5 mM). After 1 to 4 days for nAChR expression, oocytes were used for recording or confocal microscopy.

Agonist-activated nicotinic receptor responses were measured by two-electrode voltage clamp recording using a GeneClamp 500 (Molecular Devices; Sunnyvale, CA) voltage clamp. Electrodes were constructed from Kwik-Fil borosilicate glass capillary tubes (1B150F-4; World Precision Instruments, Inc.; Sarasota, FL) using a programmable microelectrode puller (P-87; Sutter Instrument Co.; Novato, CA). The electrodes had tip resistances of 0.8–2.0 MΩ after filling with 3 M KCl. During recording, oocytes were superfused with Ca^{2+}-free ND-96 via bath-application and laminar-flow microperfusion using a computer-controlled application and washout system (SF-77B; Warner Instruments; Hamden, CT; (Drenan et al., 2005)). The holding potential was -50 mV, and ACh was diluted in Ca^{2+}-free ND-96 and applied to the oocyte for 2-10 sec followed by rapid washout. Data were sampled at 200 Hz and low-pass filtered at 10 Hz using the GeneClamp 500 internal low-pass filter. Membrane currents from voltage clamped oocytes were digitized (Digidata 1200 acquisition system; Molecular Devices) and stored on a PC running pCLAMP 9.2 software (Molecular Devices). Concentration-response curves were constructed by recording nicotinic responses to a range of agonist concentrations (six to nine doses) and for a minimum of six oocytes. EC_{50} and Hill coefficient values were obtained by fitting the concentration-response data to the Hill equation. All data are reported as mean $\pm$ SEM.

Molecular Pharmacology Fast Forward. Published on October 11, 2007 as DOI: 10.1124/mol.107.039180
This article has not been copyedited and formatted. The final version may differ from this version.

Whole-Cell Patch Clamp Electrophysiology - N2a cells expressing YFP-labeled nicotinic receptors were visualized with an inverted microscope [Olympus IMT-2, DPlan 10X 0.25 numerical aperture (NA) and MPlan 60X 0.70 NA] under fluorescence illumination (Hg lamp). Patch electrodes (3–6 MΩ) were filled with pipette solutions containing (in mM): 88 KH_2PO_4, 4.5 $MgCl_2$, 0.9 EGTA, 9 HEPES, 0.4 $CaCl_2$, 14 creatine phosphate (Tris salt), 4 Mg-ATP, 0.3 GTP (Tris salt), pH 7.4 with KOH. The extracellular solution (ECS) was (in mM): 150 NaCl, 4 KCl, 2 $CaCl_2$, 2 $MgCl_2$, 10 HEPES, and 10 D-glucose, pH 7.4. Standard whole-cell recordings were made using an Axopatch 1-D amplifier (Molecular Devices), low-pass filtered at 2–5 kHz, and digitized on-line at 20 kHz (pClamp 9.2; Molecular Devices). Series resistance was compensated 80%, and the membrane potential was held at -70 mV. Recorded potentials were corrected for junction potential.

ACh was delivered using a two-barrel glass theta tube (outer diameter ~200 μm; pulled from 1.5 mm diameter theta borosilicate tubing) connected to a piezoelectric translator (Burleigh LSS-3100; Fishers, NY) as previously described (Nashmi et al., 2003). ACh was applied for 500 msec (triggered by pCLAMP 9.2) and solution exchange rates measured from open tip junction potential changes during application with 10% ECS were typically ~300 μsec (10–90% peak time). Data are reported as mean ± SEM for the peak current response to 1 μM ACh, and statistical significance was determined using a Wilcoxon signed-rank test.

Molecular Pharmacology Fast Forward. Published on October 11, 2007 as DOI: 10.1124/mol.107.039180
This article has not been copyedited and formatted. The final version may differ from this version.

Results

Design and Construction of α6 and β3 XFP fusions - Based on previous work (Nashmi et al., 2003; Slimko et al., 2002), we chose to insert XFP fusions in the M3-M4 loop of mouse α6 and β3 nAChR subunits. Like all members of the Cys-loop family, α6 and β3 have predicted α-helices at the N and C terminal ends of their M3-M4 loop (Figure 1A and 1B) that may be important in ion permeation (Miyazawa et al., 1999). In addition to avoiding these regions, we also avoided potential phosphorylation sites and trafficking motifs (Figure 1A and 1B). Our XFP fusion cassette also consisted of a Gly-Ala-Gly flexible linker flanking the XFP open reading frame on both the N and C-terminal side. We built three independent XFP fusions for α6 and two XFP fusions for β3 (Figure 1C). These were designated according to the residue immediately N-terminal to the beginning of the Gly-Ala-Gly linker (example: α6-YFP^{G366} denotes that the GAG-YFP-GAG cassette was inserted between G366 and V367). Unless otherwise noted, all experiments were conducted with α6-XFP^{A405} and β3-XFP^{P379}.

Functional Expression of α6 and β3 subunits - Despite exhaustive attempts to functionally reconstitute α6* nAChRs in *Xenopus* oocytes and mammalian tissue culture cells, we recorded no robust, reproducible responses from cells expressing α6, either with untagged subunits or the fluorescent subunits (Supplemental Data, Table 1). β3-YFP, however, was well-expressed on the plasma membrane of *Xenopus* oocytes when co-expressed with α3 and β4 subunits to support functional expression (Figure 2A). As a control for oocyte autofluorescence, we imaged oocytes expressing untagged β3 subunits

Molecular Pharmacology Fast Forward. Published on October 11, 2007 as DOI: 10.1124/mol.107.039180
This article has not been copyedited and formatted. The final version may differ from this version.

(Figure 2A). No fluorescence was detected in this case, indicating that our β3-YFP signal was specific.

β3 subunits do not drastically alter the EC_{50} for ACh or nicotine when incorporated into nAChRs (Boorman et al., 2003), but do profoundly alter single channel kinetics (Boorman et al., 2003). Channel burst duration was significantly shortened for nAChRs containing β3 versus those without it (Boorman et al., 2003), suggesting that β3 reduces the probability of channel opening, P_{open}. Consistent with this, macroscopic voltage-clamped responses from oocytes and mammalian cells expressing β3* receptors were significantly smaller than for non-β3* receptors (Broadbent et al., 2006). To asses the functionality of our β3-YFP construct, we compared the ability of untagged and YFP-labeled β3 subunits to attenuate nicotinic responses. β3 must be co-expressed with other α and β subunits, so we chose to use α3β4 receptors for this purpose. We did so because β3 has been the well-characterized with this receptor combination (Boorman et al., 2003; Broadbent et al., 2006). When WT, untagged β3 was co-expressed with α3β4 receptors, we found a significant attenuation of the peak response to 200 μM ACh (Figure 2B), consistent with previous findings (Broadbent et al., 2006). When β3-YFP was tested in this assay, it was also able to attenuate the maximal response in a manner identical to untagged β3 (Figure 2B). It is possible that, while WT β3 attenuates responses via a gating mechanism on the plasma membrane, YFP-labeled β3 might do so via a different mechanism such as sequestering α3 or β4 subunits inside the cell. To further test the functionality of YFP-labeled β3, we took advantage of the fact that a gain-of-function TM2 mutation in β3 is able to reverse the attenuation of peak responses seen for WT β3

Molecular Pharmacology Fast Forward. Published on October 11, 2007 as DOI: 10.1124/mol.107.039180
This article has not been copyedited and formatted. The final version may differ from this version.

(Broadbent et al., 2006). We reasoned that, if the YFP label in the M3-M4 loop is not disturbing the function of β3, we should detect the same gain-of-function response for unlabeled and YFP-labeled β3 when they are engineered to express a mutation of this sort. When a Val13' to Ser mutation (V13S) was introduced into unlabeled β3, we observed not only a reversal of this attenuation behavior, but a significant increase in the peak response to 200 μM ACh with α3β4 receptors (Figure 2C). When β3-YFP^{V13S} was tested in this assay, we observed an identical behavior. Taken together, these data suggest that β3-YFP is fully functional and incorporates into nAChRs in *Xenopus* oocytes.

To further characterize our β3-YFP construct, we constructed concentration-response curves for α3β4 receptors containing either β3 WT or β3-YFP. Consistent with previous reports (Boorman et al., 2000), we measured an EC_{50} for ACh of 230 $\pm$ 22 μM for α3β4β3 receptors, which is slightly higher than for α3β4 (165 $\pm$ 9 μM) (Figure 3A). When β3-YFP was substituted for WT β3, the EC_{50} was shifted slightly, but acceptably, to 109 $\pm$ 8 μM (Figure 3A). We also noticed that the addition of β3 to α3β4 receptors increased the Hill coefficient from 1.5 $\pm$ 0.1 to 2.0 $\pm$ 0.3, and this effect was retained when β3-YFP was co-expressed with α3β4 receptors. Similarly, we also constructed concentration-response relationship curves for oocytes expressing β3^{V13S} and β3-YFP^{V13S}. Compared to the EC_{50} for α3β4β3 (230 $\pm$ 22 μM), we measured an EC_{50} for α3β4β3^{V13S} of 28 $\pm$ 3 μM (Figure 3B). This is consistent with others who have reported an approximate 6-fold reduction in EC_{50} for the inclusion of β3 with a similar hypersensitive mutation, Val9'Ser (Boorman et al., 2000). We reasoned that if β3-YFP

Molecular Pharmacology Fast Forward. Published on October 11, 2007 as DOI: 10.1124/mol.107.039180
This article has not been copyedited and formatted. The final version may differ from this version.

retained the WT function of β3, then there should be a similar gain-of-function phenotype when it is co-expressed with α3β4. We measured an EC_{50} for α3β4β3-YFP^{V13S} of 34 ± 3 μM (Figure 3B), confirming that this construct behaves identically to β3 WT. Collectively, our work in *Xenopus* oocytes with YFP-labeled β3 subunits suggests that insertion of YFP into the M3-M4 loop does not significantly alter the assembly, subcellular trafficking, or function of this subunit.

Subcellular localization and trafficking of α6 and β3 subunits – To probe the subcellular localization and trafficking of α6* and β3* receptors, we chose a mouse neuroblastoma cell line, N2a, to transiently express our fluorescent nicotinic receptor subunits. We prefer these cells over, for example, HEK293 cells, because they 1) are of mouse origin, the same species as our fluorescent constructs, 2) are of neuronal origin, suggesting that they will be a permissive environment for correct expression, subcellular localization, and assembly of our ectopic nAChR subunits 3) express only moderate quantities of transfected membrane protein. To study the subcellular localization of β3* receptors, we co-expressed β3-YFP with the previously described fluorescently-labeled α4 and β2 subunits (Nashmi et al., 2003). β3 is able to assemble and function when co-expressed with α4β2 receptors (Broadbent et al., 2006). When co-expressed with fluorescent α4 or β2 receptors, β3-YFP was localized primarily in the endoplasmic reticulum (ER) of live N2a cells (Figure 4A, panel i and 4B, panel i). We utilized CFP-labeled α4 (Figure 4B, panel ii) or β2 (Figure 4A and C, panel ii) subunits along with a confocal microscope with spectral imaging capabilities to unambiguously assign YFP and CFP signals to each pixel for the spectral images of the cells. In these experiments, YFP was assigned green,

Molecular Pharmacology Fast Forward. Published on October 11, 2007 as DOI: 10.1124/mol.107.039180
This article has not been copyedited and formatted. The final version may differ from this version.

CFP was assigned red, and yellow indicated pixels where β3-YFP was co-localized with either β2-CFP (Figure 4A, panel iii) or α4-CFP (Figure 4B, panel iii). We noted that β3-YFP was completely co-localized with either α4 or β2 in this experiment, suggesting that these subunits are assembled in the same pentameric receptors. To further define the extent of this co-localization, we plotted the β3-YFP and α4-CFP or β2-CFP pixel intensity across a two-dimensional region of interest transecting the cell (Figure 4A and B, panel iv). We noted that the YFP and CFP intensity profiles strongly resembled each other, suggesting that these subunits were indeed co-localized and co-assembled in intracellular compartments of the cell. With respect to α4β2* receptors, this localization pattern is not an artifact of overexpression, as this is the same pattern we observed previously (Nashmi et al., 2003). This is also the expression pattern of endogenous, YFP-labeled α4* receptors in α4-YFP knock-in mice (Nashmi et al., 2007). This indicates that 1) a large pool of intracellular receptors exists in neurons, and 2) YFP tag does not interfere with the delivery of receptors to the plasma membrane. Thus, the localization pattern we observe here for β3 subunits is the expected result if it is assembling with α4β2 receptors.

We expressed α6-YFP along with β2-CFP in N2a cells and analyzed its localization pattern as described above for β3. We also found that α6 was localized in intracellular compartments in the cell (Figure 4C, panel i), and that it was completely co-localized with β2 subunits (Figure 4C, panel ii to iv). Although this is the first fluorescence imaging reported for α6* receptors, there is other evidence to corroborate our findings. Studies with [^{3}H]-epibatidine demonstrate that a significant portion of

Molecular Pharmacology Fast Forward. Published on October 11, 2007 as DOI: 10.1124/mol.107.039180
This article has not been copyedited and formatted. The final version may differ from this version.

α6β2 and α6β2β3 receptors are intracellular (~50% and ~20%, respectively), although some are delivered to the surface (Kuryatov et al., 2000; Tumkosit et al., 2006).

To further investigate the subcellular localization and trafficking of α6 and β3 subunits, we imaged live, differentiated N2a cells and primary neurons. N2a cells can be induced to differentiate and undergo neurite outgrowth if serum is withdrawn and an activator of PKA, dibutyryl-cAMP, is added (Fowler et al., 2001). In our previous work, α4β2 receptors were localized to dendrites, but not axons, when expressed in primary midbrain neurons (Nashmi et al., 2003). We were interested in whether our fluorescent nicotinic receptor subunits were localized to N2a cell processes in a manner analogous to dendrites in primary neurons. Further, we wanted to address the question of whether β3 is localized with other subunits at distal sites such as dendrites. This is an unsolved question, as there is no high-affinity probe (pharmacological or immunological) that can reliably and unambiguously isolate β3* receptors. N2a cells were plated on glass-bottom dishes, and were then differentiated for two days (see Materials and Methods) followed by transfection with various combinations of YFP-labeled and unlabeled nAChR subunits. Cells were also co-transfected with an expression plasmid for soluble CFP to mark total cell morphology. We found that α4β2 receptors were indeed localized to neuronal processes in differentiated N2a cells (Figure 4D, arrow), along with abundant expression in the cell soma. When β3-YFP was co-expressed with α4β2, we observed a very similar pattern. We found that β3 was present even at the most distant elements of neuronal processes (Figure 4D, arrow). Because this pattern is identical to that of α4β2 in differentiated N2a cells, we conclude that β3 is likely assembling with α4β2 receptors, and that the YFP label in the M3-M4 loop is not disrupting the normal cellular trafficking

Molecular Pharmacology Fast Forward. Published on October 11, 2007 as DOI: 10.1124/mol.107.039180
This article has not been copyedited and formatted. The final version may differ from this version.

of α4β2β3 pentamers. To further characterize the localization of β3* receptors, we co-expressed β3-YFP with α4β2 receptors in primary rat hippocampal neurons (Nashmi et al., 2003). To minimize overexpression artifacts, cells were imaged live only 18-24 hours after transfection. We found that β3* receptors were localized very similarly to α4β2 receptors in our previous studies with primary neurons; we noted uniform localization in the soma, suggestive of endoplasmic reticulum, as well as dendritic localization (Figure 5A, arrow) and an absence of localization in axons. A high magnification micrograph demonstrates the dendritic localization of these putative α4β2β3 receptors (Figure 5A, right panel). In cells co-expressing α4/β2/β3Y with soluble CFP (to mark total cell morphology, similar to (Nashmi et al., 2003)), β3 subunits did not traffic to a sub-region of the cell interior likely to be axons (data not shown). To more directly determine whether β3* receptors could be localized to axons in these neurons, we co-expressed α4β2β3Y receptors with a CFP-labeled axonal marker, tau. Tau-CFP decorated axons in hippocampal neurons, with proximal (relative to the cell body) portions of the axon being labeled more strongly than distal portions (Figure 5B). In all cells examined, we noted the presence of YFP-labeled β3 subunits in these proximal axons but not distal axons (Figure 5B, arrow). These data in differentiated N2a cells and primary neurons suggest that β3 assembles efficiently with α4β2 receptors, and is thus co-trafficked and targeted to distal sites in neurons.

Because α6-YFP* receptors do not function in our hands, we wanted to determine whether this is due to a subtle trafficking defect that could prevent the correct delivery of α6-YFP to the plasma membrane. Although we could readily detect α6 fluorescence in the cell body of undifferentiated N2a cells, we wanted to further probe the cellular

Molecular Pharmacology Fast Forward. Published on October 11, 2007 as DOI: 10.1124/mol.107.039180
This article has not been copyedited and formatted. The final version may differ from this version.

trafficking of α6* receptors by expressing them in differentiated N2a cells which contain processes. To evaluate the subcellular localization of α6* receptors, we expressed α6-YFP with β2 in differentiated N2a cells. To our surprise, we found that α6β2 receptors were trafficked to neuronal processes in a manner analogous to α4β2 and α4β2β3 receptors (Figure 4D, arrow). To further address this question, we expressed α6-YFPβ2 receptors in rat hippocampal neurons as described for α4β2β3-YFP. We observed a localization pattern for α6-YFP that was very similar to α4β2β3-YFP. These receptors were well expressed in the cell soma, but were readily detectable in dendrites as well (Figure 5A, arrow). In experiments with co-expressed soluble CFP and α6-YFPβ2 receptors, α6 subunits were not detected in putative axons (data not shown). In tau-CFP / α6-YFPβ2 co-expression experiments, α6 subunits (similar to α4β2 but not α4β2β3 receptors) were not detected in tau-labeled axons (Figure 5B, arrow). These data indicate that, although α6* receptors produce little or no agonist-induced conductance in mammalian tissue culture cells, they are expressed well and trafficked similarly compared to α4β2 and β3* receptors.

FRET reveals assembly of α6 and β3 subunits into nAChR pentamers – The fact that α4/β2/β3 and α6/β2 subunits are co-localized in the cell body and co-targeted to processes and dendrites in neurons suggests that they are assembled into pentameric receptors. The question of receptor assembly is often answered by simply measuring agonist-induced conductance increases in cells expressing a subunit combination of interest, or by applying a selective agonist or inhibitor to a pure receptor population of known pharmacological properties. This approach is not applicable, however, for α6*

Molecular Pharmacology Fast Forward. Published on October 11, 2007 as DOI: 10.1124/mol.107.039180
This article has not been copyedited and formatted. The final version may differ from this version.

and β3* receptors. α6* receptors do not function well in heterologous expression systems, so it is not straightforward to determine the extent to which free α6 subunits assemble into pentameric receptors. Similarly for β3, although it is functional in oocytes (Figure 2), there are no pharmacological probes that can be applied to β3* receptors to study their assembly or subunit composition. Others have indirectly measured receptor assembly of nicotinic subunits by using biochemical techniques such as immunoprecipitation (Champtiaux et al., 2003; Zoli et al., 2002) and centrifugation (Kuryatov et al., 2000), or by forcing subunits to assemble by using molecular concatamers (Tapia et al., 2007). To directly determine whether two nicotinic receptor subunits interact and, possibly, assemble to form pentameric receptors, we have used Förster resonance energy transfer (FRET) coupled with our CFP and YFP-tagged receptors. In the context of our nicotinic receptor subunits labeled with YFP or CFP in the M3-M4 loop, only subunits that interact will undergo FRET, as FRET occurs only when donors and acceptors are within 100 Å. Furthermore, we previously demonstrated that the efficiency of FRET directly correlates with the number of functional, plasma-membrane localized pentameric receptors (Nashmi et al., 2003). To measure FRET between subunits, we employed the acceptor photobleaching method (Nashmi et al., 2003). In this method, we measure CFP dequenching during incremental photodestruction of YFP. CFP was excited with at 439 nm, while YFP was bleached at 514 nm (Figure 6A). Because the emission spectra for CFP and YFP overlap significantly, we imaged using a confocal microscope with spectral imaging capabilities along with a linear unmixing algorithm (described in Materials and Methods).

Fluorescent α4 and β2 subunits are functional and undergo robust FRET in mammalian cells (Nashmi et al., 2003), so we used these subunits in our acceptor photobleaching assay with XFP-tagged β3 and α6. We expressed β3-YFP with untagged α4 and β2-CFP in N2a cells, followed by live cell FRET imaging. We recorded the whole-cell fluorescence intensity for β3-YFP and β2-CFP before and after photobleaching of YFP with the 514 nm laser, and expressed with pseudocolor intensity scaling (Figure 6B). In this experiment, β2-CFP was clearly de-quenched after β3-YFP photodestruction (Figure 6B), indicating that the two subunits had been undergoing FRET. In a similar experiment, we recorded multiple spectral images at several time points during YFP photodestruction. This revealed a corresponding increase in CFP intensity (Figure 6C). A reciprocal experiment was also done, where β3-YFP was co-expressed with α4-CFP and untagged β2. We recorded a similar de-quenching for α4-CFP after YFP photobleaching (Figure 6D and E), indicating FRET between these subunits as well. Both for β2/β3 and α4/β3 FRET, we found no difference between FRET inside the cell versus FRET at the cell periphery at or near the plasma membrane. These results directly demonstrate that β3 is able to assemble with α4β2 receptors in neuronal cells. This assembly likely occurs in the endoplasmic reticulum, which is consistent with previous findings (Nashmi et al., 2003).

There are many different putative α6* receptor subtypes in brain, including α6β2, α6β2β3, α6α4β2, and α6α4β2β3 (Salminen et al., 2007). To begin to study α6* receptor assembly, we measured FRET between α6-YFP and β2-CFP. In response to YFP bleaching, we recorded a robust de-quenching of β2-CFP throughout the cell,

Molecular Pharmacology Fast Forward. Published on October 11, 2007 as DOI: 10.1124/mol.107.039180
This article has not been copyedited and formatted. The final version may differ from this version.

indicating FRET between these subunits (Figure 6F and G). The pattern of localization and FRET pattern was identical to α4β2β3 receptors.

To further quantify FRET between α4/β2 subunits and β3 or α6, we measured FRET *E* values for various receptor subtypes. α4-CFPβ2-YFP, α4β2-CFPβ3-YFP, and α4-CFPβ2β3-YFP receptors were expressed in N2a cells followed by acceptor photobleaching FRET (Figure 7A). We acquired spectral images with 439 nm laser excitation before and during incremental photobleaching of YFP-labeled subunits, followed by extraction of true CFP and YFP image data using linear unmixing (see Materials and Methods). A scatterplot of CFP intensity in response to YFP photobleaching reveals FRET between the subunits in question (Figure 7B) when the slope of the linear regression line is > 0. This slope was used to calculate FRET efficiency values, which were expressed as bar graphs (Figure 7C) or listed (Table 1). As shown qualitatively in Figure 6, significant FRET occurred in all nAChR pentamer conditions. We noted a higher FRET *E* for α4C/β2Y than for β3Y with either β2C or α4C ("Y" = YFP, "C" = CFP). To asses the specificity of this measurement, we also measured FRET between β3 and a non-nAChR, CFP-labeled protein, mGAT1. GAT1 is also a multipass transmembrane protein with a CFP-tag at its C-terminus, which faces the cytoplasm. This protein is mainly localized to the endoplasmic reticulum (data not shown). These two points are important, as it was critical for a specificity probe to have 1) the same membrane topology as our labeled nicotinic receptors, with respect to the attached fluorophore, and 2) the same subcellular localization such that they are capable of interacting with each other. In N2a cells expressing β3-YFP and mGAT1-CFP, we could not detect any FRET between these proteins (Table 1, Figure 7C). In an even more

Molecular Pharmacology Fast Forward. Published on October 11, 2007 as DOI: 10.1124/mol.107.039180
This article has not been copyedited and formatted. The final version may differ from this version.

rigorous test, we assessed FRET between β3-YFP and another Cys-loop receptor labeled in the M3-M4 loop, the CFP-labeled GluCl β subunit (Nashmi et al., 2003; Slimko et al., 2002). FRET between β3 and the GluCl β subunit was significantly smaller (FRET *E* = 6 ± 4 %) than for α4 or β2 nAChR subunits (Table 1, Figure 7C). Thus, our FRET results between β3 and other labeled nAChR subunits cannot be explained by random collision or interaction with unassembled subunits. Finally, we were interested in whether subtle changes in the location of the fluorophore within the β3 M3-M4 loop could influence its ability to undergo FRET with another subunit. FRET *E* is thus roughly proportional to the distance between fluorophores. We reasoned that changes in the insertion point of YFP in β3, while holding the position of CFP in β2 constant, might alter FRET between these two subunits To address this, we compared the FRET *E* between β2-CFP and two different β3-YFP constructs, β3-YFP^{P379} and β3-YFP^{G367}, which have different insertion points for YFP within the M3-M4 loop. To our surprise, there was no change in the FRET *E* for these two subunits (Table 1, Figure 7D).

We quantitatively measured FRET between α6 and α4/β2 subunits as well. We expressed either α6Yβ2C, or α6Yα4Cβ2 in N2a cells in order to measure FRET (Figure 8A). The latter receptor was studied because recent work indicates that nAChR receptors containing both α6 and α4 1) exist and are functional in mouse brain tissue (Salminen et al., 2007), and 2) are both necessary to form the nAChR subunit with the highest affinity for nicotine yet reported (Salminen et al., 2007). Acceptor photobleaching FRET experiments reveal robust CFP dequenching in response to YFP photobleach for both of these receptor subtypes, indicating FRET (Figure 8B). Similar to β3-YFP* receptors, we measured FRET *E* values for these two subtypes, and found a FRET *E* of 36.0 ± 2.4 %

Molecular Pharmacology Fast Forward. Published on October 11, 2007 as DOI: 10.1124/mol.107.039180
This article has not been copyedited and formatted. The final version may differ from this version.

for α6Yβ2C, and 21.9 ± 1.1 % for α6Yα4Cβ2 (Table 1, Figure 8C). We also assessed the specificity of our FRET measurements for α6 by measuring FRET between α6-YFP and mGAT1-CFP as described above for Figure 7. Similar to β3 and mGAT1, we could record no significant FRET between α6 and mGAT1 (Table 1, Figure 8C). FRET experiments between α6 and the GluCl β subunit, the most rigorous test conducted, yielded a small FRET signal (FRET E = 14 ± 2 %) (Table 1, Figure 8C). Because these subunits presumably do not form functional channels, there may be a small distortion of our α6 FRET signals that is due to partially assembled receptors. Because this signal is significantly smaller than for all other α6 combinations, FRET between subunits in pentameric receptors remains the most plausible explanation for the energy transfer we observe for α6. Finally, we studied FRET between β2-CFP and three α6-YFP constructs (α6-YFP^{A405}, α6-YFP^{G387}, and α6-YFP^{G366}) that differed only in their insertion point for YFP within the M3-M4 loop. Again, we were surprised to find no significant difference in FRET E between these three α6 constructs (Table 1, Figure 8D).

Several results described above gave us confidence that our XFP-labeled β3 and α6 constructs were performing as expected. After confirming that these subunits assemble and traffic normally when expressed independently of each other, we used these constructs together to study α6β2β3 nAChRs. This receptor represents a modest population of the total striatal nAChR pool, and contributes to nicotine-stimulated DA release (Salminen et al., 2007). α6β2β3 receptors, where one subunit is untagged and the remaining subunits are either YFP or CFP-tagged (α6Yβ2Cβ3, α6Yβ2β3C, and α6β2Yβ3C), were expressed in N2a cells (Figure 9A). We measured robust donor

dequenching for all receptor subtypes (Figure 9B), which was confirmed with FRET *E* measurements (Table 1, Figure 9C). Thus, aside from α6 functional measurements, we conclude that XFP-labeled α6 and β3 subunits exhibit normal subcellular trafficking and assembly when compared to our well-characterized fluorescent α4 and β2 subunits.

α6 and β3 subunit stoichiometry probed with FRET – Having established that fluorescently-labeled α6 and β3 are functional (β3 only), have a reasonable subcellular localization pattern, and assemble into nicotinic receptor pentamers with other subunits, we used these tools to probe an important question facing the nicotinic receptor field: subunit stoichiometry. A variety of creative approaches have been taken to understand subunit stoichiometry, including immunoprecipitation (Champtiaux et al., 2003; Zoli et al., 2002), density gradient centrifugation (Kuryatov et al., 2000), molecular concatamers/linked subunits (Tapia et al., 2007), reporter mutations (Boorman et al., 2000), and mouse genetic approaches (Gotti et al., 2005a; Salminen et al., 2007). We now use FRET to address the problem of subunit stoichiometry because FRET occurs only when subunits are directly interacting, and often assembled, with one another.

We have previously shown that FRET efficiency correlates directly with functional receptor pentamers (Nashmi et al., 2003). To examine the number of α6 and β3 subunits in a nicotinic receptor pentamer, we first used FRET to examine the stoichiometry of a well-studied receptor, namely α4β2 receptors. It is widely accepted that α4 and β2 subunits assemble to form both high-sensitivity (HS) and low-sensitivity (LS) receptors. Cells often produce a mixture of these two receptors (Buisson and Bertrand, 2001; Nashmi et al., 2003), although they can be induced to express a pure

Molecular Pharmacology Fast Forward. Published on October 11, 2007 as DOI: 10.1124/mol.107.039180
This article has not been copyedited and formatted. The final version may differ from this version.

population of one or the other (Briggs et al., 2006; Nelson et al., 2003). The subunit stoichiometry of HS receptors is postulated to be $(\alpha4)_2(\beta2)_3$, whereas the LS receptors is thought to be $(\alpha4)_3(\beta2)_2$ (Nelson et al., 2003). Regardless of the fraction of HS and LS receptors, we took advantage of the fact that all α4β2 receptors presumably contain ≥ two α4 and ≥ two β2 subunits. We reasoned that when cells express α4-YFP and α4-CFP along with β2 (Figure 10A), a fraction of the receptors will contain both YFP and CFP-labeled α4 subunits, and will therefore be detectable by FRET. Confirming this hypothesis, we did detect modest de-quenching of α4-CFP upon incremental α4-YFP photobleaching (Figure 10B). FRET *E* for α4Yα4Cβ2 receptors was 22.2 ± 2.3 % (Table 1, Figure 10C). We also conducted a similar experiment with β2, and found a modest FRET signal (FRET *E* = 16.3 ± 1.7 %) between β2-YFP and β2-CFP within the same pentamer (Table 1, Figure 10B and C). We next used this assay to determine whether or not α6* and β3* receptors have one or more than one α6 or β3 subunit per pentamer. N2a cells expressing either α6Yα6Cβ2 or α4β2β3Yβ3C receptors were analyzed for FRET (Figure 10A). We measured a strong FRET signal between α6-YFP and α6-CFP in donor de-quenching (Figure 10B), corresponding to a robust FRET *E* of 27.8 ± 1.7 % (Table 1, Figure 10C). Thus, these data are the first to directly demonstrate that α6* receptors are capable of containing at least two α6 subunits, similar to other α subunits such as α3 and α4. In contrast to α6, β3 is thought to be an "ancillary subunit", only able to incorporate into nAChRs with other α and β subunits (Groot-Kormelink et al., 1998). We could detect little or no FRET between β3-YFP and β3-CFP (FRET *E* = 2.6 ± 1.3 %) (Table 1, Figure 10B and C). This was a specific result, as β3-YFP and β3-

CFP were able to FRET with other subunits (Figure 7 and 9), thus ruling out the notion that one of these subunits is not able to undergo FRET. These data are the first to directly demonstrate that receptors containing β3 subunits are only able to incorporate a single copy of this subunit. We interpret this to mean that β3 incorporates into the "accessory" position in a nAChR pentamer (Tumkosit et al., 2006), and likely does not contribute to either of the two α:non-α interfaces that form the ligand-binding sites.

After confirming via FRET that β3 incorporates into nAChRs at a frequency of one subunit per pentamer, we used β3 co-expression to further probe the subunit stoichiometry of α4* and α6* receptors. We co-expresssed WT β3 with α4-YFP, α4-CFP, and β2 such that β3 was in excess. In this experiment, β3 is incorporated into α4-XFPβ2 receptors and will displace either an α4 or β2 subunit. There was a significant decline in FRET for cells expressing α4Yα4Cβ2β3 receptors versus those expressing α4Yα4Cβ2 (Table 1, Figure 10D and G). We interpret this result to mean that β3 incorporation has fixed the subunit stoichiometry of FRET-competent receptors to $(\alpha4Y)_1(\alpha4C)_1(\beta2)_2(\beta3)_1$, versus the following mixture of FRET-competent receptors without β3: $(\alpha4Y)_2(\alpha4C)_1(\beta2)_2$, $(\alpha4Y)_1(\alpha4C)_2(\beta2)_2$, and $(\alpha4Y)_1(\alpha4C)_1(\beta2)_3$. A reduction in FRET for two XFP-labeled α4 subunits (YFP and CFP) versus three is reasonable and expected based on the work of others (Corry et al., 2005), and on our calculations that predict the relative FRET efficiencies in pentamers with XFP-labeled subunits (data not shown). Thus, β3 incorporation into nAChR pentamers likely displaces one subunit, and results in a decrease in α4 to α4 FRET for pentamers with a mixed subunit stoichiometry.

Molecular Pharmacology Fast Forward. Published on October 11, 2007 as DOI: 10.1124/mol.107.039180
This article has not been copyedited and formatted. The final version may differ from this version.

To determine whether α6* receptors have a fixed or a mixed subunit stoichiometry, we co-expressed β3 in excess with α6-YFP, α6-CFP, and β2. If α6* receptors only incorporate two α6 subunits, we expect to observe little or no change in FRET between α6-YFP and α6-CFP because β3 will only displace one unlabeled β2 subunit. However, if α6* receptors exist as a mixture of $(\alpha6)_2(\beta2)_3$ and $(\alpha6)_3(\beta2)_2$ subtypes similar to α4* receptors, we expect to observe a similar decline in FRET when β3 is present to induce only the $(\alpha6)_2(\beta2)_2\beta3$ stoichiometry. The latter was the case. We noted a significant decline in the slope of the donor de-quenching profile for α6Yα6C* receptors when β3 was present (Table 1, Figure 10E), and a decline in the FRET *E* for α6Yα6Cβ2β3 (21.7 ± 1.4 %) versus α6Yα6Cβ2 (27.8 ± 1.7 %) (Table 1, Figure 10G). Thus, fluorescent α6* receptors behave identically to α4* receptors, and these results suggest that α6* receptors are capable of forming either of two subunit stoichiometries: $(\alpha6)_2(\beta2)_3$ and $(\alpha6)_3(\beta2)_2$.

Several groups have reported the existence of α4α6* receptors in brain tissue (Salminen et al., 2007; Zoli et al., 2002), and α4α6β2β3* receptors (presumably $\alpha4_1\alpha6_1\beta2_2\beta3_1$) have high affinity for nicotine (Salminen et al., 2007). To learn about the subunit stoichiometry of α4α6* receptors, we expressed α6-YFP and α4-CFP along with β2 subunits in N2a cells. We noted a modest FRET signal, indicating that these subunits are present in some of the same nicotinic receptor pentamers (Figure 8B and C, Figure 10F). In contrast to our results with α6β2β3 and α4β2β3 receptors, there was no difference between cells transfected with α6Y/α4C/β2 and α6Y/α4C/β2/β3 subunits (Figure 10F and G). This shows that addition of excess β3 subunits did not reduce FRET

Molecular Pharmacology Fast Forward. Published on October 11, 2007 as DOI: 10.1124/mol.107.039180
This article has not been copyedited and formatted. The final version may differ from this version.

between α6Y and α4C. Thus, this experiment is not informative regarding α4α6β2β3 receptors in N2a cells. For instance, the α:β subunit stoichiometry as measured by FRET may not change in the presence of β3.

TIRF reveals α4,α6*, and β3* receptor plasma membrane localization* – Having confirmed that fluorescent α6 and β3 subunits assemble to form nicotinic receptor pentamers, we probed the plasma membrane localization of nAChRs containing these subunits using total internal reflection fluorescence (TIRF) microscopy. For nicotinic receptor subunits fused to fluorescent proteins, TIRF illumination selectively excites only receptors at or very close to the plasma membrane. We imaged live N2a cells expressing α4β2β3-YFP, α6-YFPβ2, and α4-YFPβ2. In epifluorescence mode (Figure 11, "epi" panels), these receptors exhibited an intracellular, endoplasmic reticulum-like localization identical to our confocal imaging data in Figure 4. In TIRF mode, however, we noted robust plasma membrane fluorescence for all receptor combinations. Surprisingly, we found α4Yβ2 receptors to be localized to distinct, filamentous structures protruding from the cell body (Figure 11A, arrow). This specific filamentous pattern was seen for > 90% of the plasma membrane fluorescence. These structures were reminiscent of filopodia, which are actin-dependent plasma membrane protrusions. To test whether these structures contain actin, a hallmark of filopodia, we imaged cells stained with rhodamine-phalloidin, a marker of polymerized actin. We noted distinct, actin-containing protrusions (Figure 11B, arrow). These structures were actin-dependent, as they were destroyed by treatment with latrunculin B, an actin-disrupting agent (Figure 11B, right

Molecular Pharmacology Fast Forward. Published on October 11, 2007 as DOI: 10.1124/mol.107.039180
This article has not been copyedited and formatted. The final version may differ from this version.

panel). These data indicate that, in N2a cells, α4Yβ2 nicotinic receptors are localized to membrane protrusions that strongly resemble filopodia.

Similar to α4Yβ2, we imaged live N2a cells, in TIRF mode, expressing either α4β2β3Y or α6Yβ2. To our surprise, we noted a very different localization pattern compared to α4Yβ2. β3* and α6* receptors were well-expressed on the plasma membrane, but there was no evidence of membrane protrusion or filopodia localization for these receptors. Rather, these proteins exhibited a punctate, lattice-like localization pattern on the plasma membrane (Figure 11C and D). This pattern was consistently seen in other cells types such as HEK293 (data not shown), and suggests that β3* or α6* receptors cluster in microdomains distinct from α4β2 receptors. Alternatively, some of these puncta could be clusters of assembled receptors adjacent to the plasma membrane within the 100 nm evanescent wave. We also recorded movies to monitor plasma membrane nAChRs, and noted that, although they exhibited localized, stochastic movements, most of these receptor clusters did not travel or translocate to any significant degree (data not shown). This localization pattern resembles that of the SNARE protein syntaxin1, which was localized to distinct granules or microdomains in the plasma membrane when observed in TIRF (Ohara-Imaizumi et al., 2004). Because SNARE proteins are important regulators of ion channel subcellular trafficking and function in neuronal soma and synaptic terminals (Bezprozvanny et al., 1995), we compared the plasma membrane localization pattern of YFP-syntaxin1A with β3-YFP* and α6-YFP* receptors in N2a cells. We observed a plasma membrane distribution pattern for syntaxin1A that was very similar to β3 and α6 subunits; syntaxin1A was also localized to

Molecular Pharmacology Fast Forward. Published on October 11, 2007 as DOI: 10.1124/mol.107.039180
This article has not been copyedited and formatted. The final version may differ from this version.

distinct clusters adjacent to the plasma membrane or microdomains on the plasma membrane (Figure 11E).

It is possible that the different plasma membrane localization pattern observed for α4Yβ2 versus α4β2β3Y reflects the localization pattern of functional versus non-functional nicotinic receptors, respectively. To address this, we used whole-cell patch clamp electrophysiology to record voltage-clamped responses from functional, fluorescent nAChRs expressed in N2a cells. Because WT (Broadbent et al., 2006) or YFP-tagged β3 subunits (Figure 2B) significantly attenuated nAChR responses, we employed β3-YFP^{V13S} subunits to reverse this attenuation. We reasoned that, if co-expressed and co-assembled with α4β2 receptors, β3-YFP^{V13S} subunits should 1) induce the high-sensitivity $(\alpha4)_2(\beta2)_2(\beta3)_1$ subunit stoichiometry similar to previous work (Broadbent et al., 2006), and 2) lower the EC_{50} for activation of this high-sensitivity form by approximately one order of magnitude (Figure 3B). When voltage-clamped N2a cells expressing α4Yβ2 receptors were stimulated with 1 μM ACh, a dose which induces minimal (20-30 pA) responses in our previous work with HEK293 cells (Nashmi et al., 2003), we observed an identical phenotype (Figure 11F). Responses to 300 μM ACh were robust (200-400 pA), indicating significant plasma membrane expression of these receptors (data not shown). However, cells expressing α4β2β3Y^{V13S} receptors exhibited robust responses to 1 μM ACh (Figure 11F), which was significantly larger than the response size for α4β2 receptors (Figure 11G). This is the expected result if β3-YFP^{V13S} subunits are incorporated into functional nAChRs in N2a cells, and is consistent with our *Xenopus* oocyte experiments (Figure 2 and 3), and with the work of others (Broadbent et al., 2006). These data confirm that both α4Yβ2 and α4β2β3Y receptors are functional in

Molecular Pharmacology Fast Forward. Published on October 11, 2007 as DOI: 10.1124/mol.107.039180
This article has not been copyedited and formatted. The final version may differ from this version.

N2a cells, and that the observed plasma membrane localization pattern for functional α4Yβ2 and α4β2β3Y receptors is significantly different.

Molecular Pharmacology Fast Forward. Published on October 11, 2007 as DOI: 10.1124/mol.107.039180
This article has not been copyedited and formatted. The final version may differ from this version.

Discussion

Subcellular Localization of Nicotinic ACh Receptors – α4β2 receptors were localized intracellularly in our previous studies in HEK293 cells and primary midbrain neurons (Nashmi et al., 2003), although enough receptors are expressed on the cell surface to record responses using electrophysiology. Further, knock-in mice with YFP-labeled α4 subunits show uniform intracellular and plasma membrane localization of α4* receptors (Nashmi et al., 2007). Other investigators have found a similar localization pattern for α4β2 (Xu et al., 2006), α3β4 (Grailhe et al., 2004), α7 (Xu et al., 2006), and 5-HT_{3A} (Grailhe et al., 2004) receptors. In light of these studies, it is not surprising that we found fully assembled β3* and α6* receptors in intracellular stores in N2a cells. This suggests that neurons produce more assembled nAChRs than they can use at any particular time, and that they may require the ability to rapidly change either their total number or specific stoichiometry of receptor subtypes on the plasma membrane in response to different extracellular signals. The specific phenomenon of up or down-regulation of nicotinic receptors occurs during chronic nicotine exposure (Marks et al., 1983; Nashmi et al., 2007) and in other neurological disorders including autism and Alzheimer's disease (reviewed in (Graham et al., 2002)).

α4β2 receptors were localized to actin-dependent membrane protrusions akin to filopodia, whereas β3* and α6* receptors were not. Filopodia are critical sensory components of growth cones, influencing growth cone orientation and turning toward extracellular cues. Nicotinic receptors are required for growth cone orientation in some neuronal types (Zheng et al., 1994). Interestingly, α4 and β2 subunits are highly expressed during embryogenesis (Azam et al., 2007), suggesting a role for these subunits

Molecular Pharmacology Fast Forward. Published on October 11, 2007 as DOI: 10.1124/mol.107.039180
This article has not been copyedited and formatted. The final version may differ from this version.

in neuronal development as well as in adult function. α6 and β3 subunits, in contrast, are not expressed at appreciable levels until after birth (Azam et al., 2007). We speculate that the differences we observe for α4β2 versus β3 or α6 receptors on the plasma membrane could reflect their involvement (or lack thereof) in neuronal development.

α6 Functional Expression – Although it remains unclear why it is very difficult to record functional responses from α6* receptors, this study advances our knowledge of this problem. In 20 different attempts, using several expression/assay systems, we could record no α6 functional responses (Supplemental Data, Table 1). This could be a result of many different problems, such as α6 mRNA stability, α6 protein production, proper assembly of α6* receptors, intracellular trafficking, or plasma membrane delivery. We (herein) and others have demonstrated that cells do not have an apparent problem synthesizing α6 subunits (Kuryatov et al., 2000; Tumkosit et al., 2006), and either partial or full assembly of α6* receptors occurs in mammalian tissue culture cells and *Xenopus* oocytes (Kuryatov et al., 2000; Tumkosit et al., 2006). We found robust ectopic expression of α6-YFP subunits in tissue culture cells and in primary neurons. Furthermore, based on our FRET measurements, α6 subunits are fully capable of assembling with α4, β2, and β3 subunits in a manner indistinguishable from that of α4 and β2. These are the presumptive subunits necessary for expression of α6* receptors in vivo (Salminen et al., 2007). Assembled α6* receptors are also localized identically to α4* receptors in our experiments. Finally, and most surprisingly, we ruled out the possibility that α6* receptors are not delivered to the plasma membrane. Plasma

Molecular Pharmacology Fast Forward. Published on October 11, 2007 as DOI: 10.1124/mol.107.039180
This article has not been copyedited and formatted. The final version may differ from this version.

membrane localization for α6* receptors was identical to that of assembled, functional β3* receptors. From these data, we conclude that, although fully assembled and partially localized on the plasma membrane, α6* receptors do not yield responses in standard functional assays. This information should facilitate the design of new experimental approaches to develop robust, reproducible reconstitution of α6 function in vitro.

Because we found no difference in FRET between α4α6β2 receptors ± β3, the experiments probing the stoichiometry of α4α6β2β3 receptors are uninformative. It is possible that there are no assembled α4α6β2β3 receptors in N2a cells. We suggest that catecholaminergic or retinal ganglion cells, which are those cells in vivo that produce high levels of functional α6* receptors (Champtiaux et al., 2003; Champtiaux et al., 2002; Gotti et al., 2005b; Lena et al., 1999; Whiteaker et al., 2000; Zoli et al., 2002), express a unique protein or factor that is essential for proper function of these receptors. It is also possible that these cells are specially suited to traffic α6* and/or β3* receptors to distal axons/presynaptic terminals. Our results probing α6 and β3 axonal targeting (Figure 5B) may be negative due to differences in the cell trafficking machinery in hippocampal (α6-negative) versus catecholaminergic (α6-positive) neurons, and highlight the need for a more detailed study of α6/β3 axonal targeting in α6-positive neurons. Perhaps there is an α6-associated protein similar to other nicotinic receptor-associated proteins, such as lynx1 (Miwa et al., 1999), which remains to be characterized.

α6 and β3* Receptor Assembly and Subunit Stoichiometry* – We previously demonstrated that FRET between XFP-labeled nicotinic receptor subunits not only reveals proximity between subunits, but that increased FRET efficiency correlates with

increased assembled, functional receptors (Nashmi et al., 2003). Because we cannot measure functional responses from α6* receptors, we must draw conclusions about their behavior inferentially by comparing it to α4β2 receptors, which are functionally expressed. Using these criteria, we conclude that α6 subunits assemble with α4, β2, and β3 subunits. Furthermore, we conducted several specificity controls (FRET with GAT1C and GluCl β) that revealed that FRET between α6 or β3 and other nAChR subunits is robust and likely explained by pentameric assembly. These experiments also reveal that a sub-population of α6 subunits may be contained in partially assembled receptors. It may be this feature that precludes routine measurement of functional responses, further supporting the notion of a special factor in vivo that promotes α6* nAChR assembly and function.

We noted a slightly higher FRET efficiency for α6* versus α4* receptors in all assays reported herein. Because FRET *E* is a rough measure of distance, we speculate that this is largely due to the smaller M3-M4 intracellular loop of α6 (~136 residues) versus α4 (~270 residues). When the same XFP-labeled β2 construct is expressed with α4 versus α6, the relative distance between fluorophores, and therefore the efficiency of FRET, will be different. Although the lack of structural information about these M3-M4 loops precludes us from making any quantitative predictions or correlations with our observed FRET *E* values, we assert that, at a qualitative level, the differences in FRET *E* for α4 versus α6 are likely explained by the differences in M3-M4 loop length.

In this paper we use FRET to describe α6 and β3 subunit stoichiometry in assembled pentamers containing these subunits. Based on our data, only one β3 subunit is able to incorporate into a nicotinic receptor pentamer with other α and β subunits. It is

not clear whether β3 does so because it lacks residues required for formation of an α:β ligand-binding interface, or if it is due to specific residues in the transmembrane segments or intracellular loops. What is clear is that β3 is able to displace one subunit in a pentamer, which affords the ability to alter the subunit stoichiometry of receptors containing this subunit. Although this has been assumed based on indirect experiments (Broadbent et al., 2006), the present study is the first to directly elucidate the stoichiometry of β3* receptors.

Based on our data, α6* receptors, like α4*, are stoichiometrically heterogeneous. Previous reports using immunoprecipitation or genetic techniques have identified the specific subunits co-assembled with α6, but not their stoichiometry (Salminen et al., 2007; Zoli et al., 2002). For example, Salminen and colleagues demonstrated the existence of native α6β2, α6β2β3, and α4α6β2β3 subtypes, among others (Salminen et al., 2007). But for α6β2 receptors, how many α6 and β2 subunits are present in a given pentamer? Our FRET results suggest that a mixture of stoichiometries exist for α6* receptors. We interpret the β3-induced decline in FRET between α6Y and α6C in α6β2 receptors to mean, at least in part, that β3 is displacing a third α6 subunit and stabilizing a stoichiometry of $(\alpha6)_2(\beta2)_2(\beta3)_1$. The alternative, that α6* receptors adopt a strict $(\alpha6)_2(\beta X)_3$ stoichiometry, is less likely. Such a scenario would require that β3 is able to significantly reduce FRET between α6Y and α6C without changing α6 stoichiometry. It is more reasonable to assume that α6 is behaving similar to α4, whose stoichiometry is varied and can be altered by β3 co-expression (Broadbent et al., 2006). α6 and β3 subunits are present in α4α6β2β3 receptors in striatum and nucleus accumbens, which

have the highest affinity for nicotine of any nicotinic subtype yet reported (Salminen et al., 2007). Their localization on dopaminergic nerve terminals coupled with this high affinity for nicotine assures that they are among the first nicotinic subtypes activated during a smoking-induced bolus of nicotine. These and other high affinity receptors are important targets for smoking cessation and Parkinson's disease medications, so understanding their subunit stoichiometry is important for the rational design of small molecule modulators of nAChR function.

Molecular Pharmacology Fast Forward. Published on October 11, 2007 as DOI: 10.1124/mol.107.039180
This article has not been copyedited and formatted. The final version may differ from this version.

Acknowledgements

We thank members of the Lester laboratory for helpful advice and discussion, including Cagdas Son, Rigo Pantoja, and Fraser Moss. Special thanks to Fraser Moss and Monica Liu for help with molecular biology and Bruce Cohen for help with electrophysiology.

References

Azam L, Chen Y and Leslie FM (2007) Developmental regulation of nicotinic acetylcholine receptors within midbrain dopamine neurons. *Neuroscience* **144**(4):1347-1360.

Bezprozvanny I, Scheller RH and Tsien RW (1995) Functional impact of syntaxin on gating of N-type and Q-type calcium channels. *Nature* **378**(6557):623-626.

Bierut LJ, Madden PA, Breslau N, Johnson EO, Hatsukami D, Pomerleau OF, Swan GE, Rutter J, Bertelsen S, Fox L, Fugman D, Goate AM, Hinrichs AL, Konvicka K, Martin NG, Montgomery GW, Saccone NL, Saccone SF, Wang JC, Chase GA, Rice JP and Ballinger DG (2007) Novel genes identified in a high-density genome wide association study for nicotine dependence. *Hum Mol Genet* **16**(1):24-35.

Boorman JP, Beato M, Groot-Kormelink PJ, Broadbent SD and Sivilotti LG (2003) The effects of β3 subunit incorporation on the pharmacology and single channel properties of oocyte-expressed human α3β4 neuronal nicotinic receptors. *J Biol Chem* **278**(45):44033-44040.

Boorman JP, Groot-Kormelink PJ and Sivilotti LG (2000) Stoichiometry of human recombinant neuronal nicotinic receptors containing the β3 subunit expressed in *Xenopus* oocytes. *J Physiol* **529 Pt 3**:565-577.

Briggs CA, Gubbins EJ, Marks MJ, Putman CB, Thimmapaya R, Meyer MD and Surowy CS (2006) Untranslated region-dependent exclusive expression of high-sensitivity subforms of α4β2 and α3β2 nicotinic acetylcholine receptors. *Mol Pharmacol* **70**(1):227-240.

Broadbent S, Groot-Kormelink PJ, Krashia PA, Harkness PC, Millar NS, Beato M and Sivilotti LG (2006) Incorporation of the β3 subunit has a dominant-negative effect on the function of recombinant central-type neuronal nicotinic receptors. *Mol Pharmacol* **70**(4):1350-1357.

Buisson B and Bertrand D (2001) Chronic exposure to nicotine upregulates the human α4β2 nicotinic acetylcholine receptor function. *J Neurosci* **21**(6):1819-1829.

Champtiaux N, Gotti C, Cordero-Erausquin M, David DJ, Przybylski C, Lena C, Clementi F, Moretti M, Rossi FM, Le Novere N, McIntosh JM, Gardier AM and Changeux JP (2003) Subunit composition of functional nicotinic receptors in dopaminergic neurons investigated with knock-out mice. *J Neurosci* **23**(21):7820-7829.

Champtiaux N, Han ZY, Bessis A, Rossi FM, Zoli M, Marubio L, McIntosh JM and Changeux JP (2002) Distribution and pharmacology of α6-containing nicotinic acetylcholine receptors analyzed with mutant mice. *J Neurosci* **22**(4):1208-1217.

Corry B, Jayatilaka D and Rigby P (2005) A flexible approach to the calculation of resonance energy transfer efficiency between multiple donors and acceptors in complex geometries. *Biophys J* **89**(6):3822-3836.

Cui C, Booker TK, Allen RS, Grady SR, Whiteaker P, Marks MJ, Salminen O, Tritto T, Butt CM, Allen WR, Stitzel JA, McIntosh JM, Boulter J, Collins AC and Heinemann SF (2003) The β3 nicotinic receptor subunit: a component of α-Conotoxin MII-binding nicotinic acetylcholine receptors that modulate dopamine release and related behaviors. *J Neurosci* **23**(35):11045-11053.

Drenan RM, Doupnik CA, Boyle MP, Muglia LJ, Huettner JE, Linder ME and Blumer KJ (2005) Palmitoylation regulates plasma membrane-nuclear shuttling of R7BP, a novel membrane anchor for the RGS7 family. *J Cell Biol* **169**(4):623-633.

Fowler MJ, Flaskos J, McLean WG and Hargreaves AJ (2001) Effects of neuropathic and non-neuropathic isomers of tricresyl phosphate and their microsomal activation on the production of axon-like processes by differentiating mouse N2a neuroblastoma cells. *J Neurochem* **76**(3):671-678.

Gotti C, Moretti M, Clementi F, Riganti L, McIntosh JM, Collins AC, Marks MJ and Whiteaker P (2005a) Expression of nigrostriatal α6-containing nicotinic acetylcholine receptors is selectively reduced, but not eliminated, by β3 subunit gene deletion. *Mol Pharmacol* **67**(6):2007-2015.

Gotti C, Moretti M, Zanardi A, Gaimarri A, Champtiaux N, Changeux JP, Whiteaker P, Marks MJ, Clementi F and Zoli M (2005b) Heterogeneity and selective targeting of neuronal nicotinic acetylcholine receptor (nAChR) subtypes expressed on retinal afferents of the superior colliculus and lateral geniculate nucleus: identification of a new native nAChR subtype α3β2(α5 or β3) enriched in retinocollicular afferents. *Mol Pharmacol* **68**(4):1162-1171.

Grady SR, Murphy KL, Cao J, Marks MJ, McIntosh JM and Collins AC (2002) Characterization of nicotinic agonist-induced [^{3}H]dopamine release from synaptosomes prepared from four mouse brain regions. *J Pharmacol Exp Ther* **301**(2):651-660.

Graham AJ, Martin-Ruiz CM, Teaktong T, Ray MA and Court JA (2002) Human brain nicotinic receptors, their distribution and participation in neuropsychiatric disorders. *Curr Drug Targets CNS Neurol Disord* **1**(4):387-397.

Grailhe R, de Carvalho LP, Paas Y, Le Poupon C, Soudant M, Bregestovski P, Changeux JP and Corringer PJ (2004) Distinct subcellular targeting of fluorescent nicotinic α3β4 and serotoninergic 5-HT_{3A} receptors in hippocampal neurons. *Eur J Neurosci* **19**(4):855-862.

Groot-Kormelink PJ, Luyten WH, Colquhoun D and Sivilotti LG (1998) A reporter mutation approach shows incorporation of the "orphan" subunit β3 into a functional nicotinic receptor. *J Biol Chem* **273**(25):15317-15320.

Kuryatov A, Olale F, Cooper J, Choi C and Lindstrom J (2000) Human α6 AChR subtypes: subunit composition, assembly, and pharmacological responses. *Neuropharmacology* **39**(13):2570-2590.

Lena C, de Kerchove D'Exaerde A, Cordero-Erausquin M, Le Novere N, del Mar Arroyo-Jimenez M and Changeux JP (1999) Diversity and distribution of nicotinic acetylcholine receptors in the locus ceruleus neurons. *Proc Natl Acad Sci U S A* **96**(21):12126-12131.

Marks MJ, Burch JB and Collins AC (1983) Effects of chronic nicotine infusion on tolerance development and nicotinic receptors. *J Pharmacol Exp Ther* **226**(3):817-825.

Miwa JM, Ibanez-Tallon I, Crabtree GW, Sanchez R, Sali A, Role LW and Heintz N (1999) lynx1, an endogenous toxin-like modulator of nicotinic acetylcholine receptors in the mammalian CNS. *Neuron* **23**(1):105-114.

Miyazawa A, Fujiyoshi Y, Stowell M and Unwin N (1999) Nicotinic acetylcholine receptor at 4.6 angstrom resolution: transverse tunnels in the channel wall. *J Mol Biol* **288**(4):765-786.

Nashmi R, Dickinson ME, McKinney S, Jareb M, Labarca C, Fraser SE and Lester HA (2003) Assembly of α4β2 nicotinic acetylcholine receptors assessed with functional fluorescently labeled subunits: effects of localization, trafficking, and nicotine-induced upregulation in clonal mammalian cells and in cultured midbrain neurons. *J Neurosci* **23**(37):11554-11567.

Nashmi R, Xiao C, Deshpande P, McKinney S, Grady SR, Whiteaker P, Huang Q, McClure-Begley T, Lindstrom JM, Labarca C, Collins AC, Marks MJ and Lester HA (2007) Chronic nicotine cell specifically upregulates functional alpha4* nicotinic receptors: basis for both tolerance in midbrain and enhanced long-term potentiation in perforant path. *J Neurosci* **27**(31):8202-8218.

Nelson ME, Kuryatov A, Choi CH, Zhou Y and Lindstrom J (2003) Alternate stoichiometries of α4β2 nicotinic acetylcholine receptors. *Mol Pharmacol* **63**(2):332-341.

Ohara-Imaizumi M, Nishiwaki C, Nakamichi Y, Kikuta T, Nagai S and Nagamatsu S (2004) Correlation of syntaxin-1 and SNAP-25 clusters with docking and fusion of insulin granules analysed by total internal reflection fluorescence microscopy. *Diabetologia* **47**(12):2200-2207.

Quick M and Lester HA (1994) Methods for expression of excitability proteins in *Xenopus* oocytes. In: Ion channels of excitable cells. T. Narahashi, Ed. *Academic Press, San Diego*:261-279.

Quik M and McIntosh JM (2006) Striatal α6* nicotinic acetylcholine receptors: potential targets for Parkinson's disease therapy. *J Pharmacol Exp Ther* **316**(2):481-489.

Rowell P (2002) Effects of nicotine on dopaminergic neurotransmission. In: Nicotinic receptors in the nervous system (Levin ED, ed).51-80. Boca Raton, FL: CRC.

Salminen O, Drapeau JA, McIntosh JM, Collins AC, Marks MJ and Grady SR (2007) Pharmacology of α-Conotoxin MII-Sensitive Subtypes of Nicotinic Acetylcholine Receptors Isolated by Breeding of Null Mutant Mice. *Mol Pharmacol* **71**(6):1563-1571.

Slimko EM, McKinney S, Anderson DJ, Davidson N and Lester HA (2002) Selective electrical silencing of mammalian neurons in vitro by the use of invertebrate ligand-gated chloride channels. *J Neurosci* **22**(17):7373-7379.

Tapia L, Kuryatov A and Lindstrom J (2007) Ca^{2+} permeability of the $(\alpha4)_3(\beta2)_2$ stoichiometry greatly exceeds that of $(\alpha4)_2(\beta2)_3$ human acetylcholine receptors. *Mol Pharmacol* **71**(3):769-776.

Tumkosit P, Kuryatov A, Luo J and Lindstrom J (2006) β3 subunits promote expression and nicotine-induced up-regulation of human nicotinic α6* nicotinic acetylcholine receptors expressed in transfected cell lines. *Mol Pharmacol* **70**(4):1358-1368.

Whiteaker P, McIntosh JM, Luo S, Collins AC and Marks MJ (2000) [^{125}I]-α-Conotoxin MII identifies a novel nicotinic acetylcholine receptor population in mouse brain. *Mol Pharmacol* **57**(5):913-925.

Xu J, Zhu Y and Heinemann SF (2006) Identification of sequence motifs that target neuronal nicotinic receptors to dendrites and axons. *J Neurosci* **26**(38):9780-9793.

Zheng JQ, Felder M, Connor JA and Poo MM (1994) Turning of nerve growth cones induced by neurotransmitters. *Nature* **368**(6467):140-144.

Zoli M, Moretti M, Zanardi A, McIntosh JM, Clementi F and Gotti C (2002) Identification of the nicotinic receptor subtypes expressed on dopaminergic terminals in the rat striatum. *J Neurosci* **22**(20):8785-8789.

Molecular Pharmacology Fast Forward. Published on October 11, 2007 as DOI: 10.1124/mol.107.039180
This article has not been copyedited and formatted. The final version may differ from this version.

Footnotes

*This work was supported by grants from the Plum Foundation, NIH (DA017279, DA019375, DA009121, NS11756), and by Philip Morris International/USA. R.N. was supported by fellowships from the Elizabeth Ross Foundation, the University of California Office of the President Tobacco Related Disease Research Program (UCOP TRDRP; 10FT-0174), and NARSAD. H.J. was supported by the Austrian Science Fund (FWF; Erwin Schroedinger Fellowship J2486). R.M.D. was supported by a fellowship from UCOP TRDRP (15FT-0030), and an NIH National Research Service Award (DA021492).

Request for Reprints: Henry A. Lester, California Institute of Technology, Division of Biology M/C 156-29, Pasadena, CA 91107. E-mail: lester@caltech.edu

Molecular Pharmacology Fast Forward. Published on October 11, 2007 as DOI: 10.1124/mol.107.039180
This article has not been copyedited and formatted. The final version may differ from this version.

Legends for Figures

Figure 1. **α6 and β3 nicotinic ACh receptor constructs used in this study**. **A**. XFP insertion points in the α6 M3-M4 intracellular loop. The M3-M4 loop primary sequence of the mouse α6 nAChR subunit was analyzed for sequences predicted to be involved in forming α-helices (light grey boxes), phosphorylation sites (white boxes), or intracellular trafficking motifs (dark grey boxes); these were specifically avoided. Arrows adjacent to "XFP" indicate insertion points. The inserted XFP (YFP or CFP) protein was modified 1) to have a flexible Gly-Ala-Gly linker flanking the XFP coding sequence and 2) to lack its STOP codon. **B**. XFP insertion points in β3 M3-M4 intracellular loop. Mouse β3-XFP fusion proteins were designed similarly to α6, as indicated in *A*. **C**. α6 and β3 nAChR constructs used in this study. In addition to WT, three α6-XFP and two β3-XFP fusions were constructed. A V13'S mutation on the WT and XFP background was introduced into β3 for characterization in *Xenopus* oocytes.

Figure 2. **Fluorescently-labeled β3 subunits are functional and expressed on the cell surface in *Xenopus* oocytes**. **A**. *Xenopus* oocytes were injected with cRNA encoding WT (control) or YFP-labeled β3 (15 ng) along with α3 (2 ng) and β4 (3 ng). The oocyte surface was imaged with direct fluorescence confocal microscopy. True YFP signal was acquired by linear unmixing of the background fluorescence spectra (untagged β3 with α3β4) and a YFP reference spectra. Scale bar indicates 54 μm. **B**. Fluorescently labeled β3 subunits are indistinguishable from WT subunits in their ability to attenuate nicotinic receptor responses. A representative voltage-clamped response from *Xenopus* oocytes expressing α3β4, α3β4β3, or α3β4β3-YFP is shown. Agonist (ACh, 200 μM) was

Molecular Pharmacology Fast Forward. Published on October 11, 2007 as DOI: 10.1124/mol.107.039180
This article has not been copyedited and formatted. The final version may differ from this version.

applied and removed as indicated by the *bar*. **C**. Reversal of β3-mediated suppression of nicotinic responses is identical in untagged and YFP-labeled hypersensitive β3. Representative voltage-clamped responses from oocytes expressing α3β4, α3β4β3^{V13S}, or α3β4β3-YFP^{V13S} are shown. Agonist application is identical to *B*.

Figure 3. **β3 nAChR subunit function is not affected by XFP insertion in M3-M4 loop**. **A**. Concentration-response relations for WT and fluorescently-labeled β3-containing receptors are similar. *Xenopus* oocytes expressing the indicated receptor subunits were voltage-clamped during agonist application and washout. Peak responses to the indicated ACh concentration were normalized and the data were fitted to the Hill equation. **B**. Concentration-response relation for β3 subunits with a hypersensitive mutation is not affected by the presence of YFP in the M3-M4 loop. *Xenopus* oocytes were assayed and data analyzed as in *A*. α3β4 data from *A* are shown for comparison. Error bars are $\pm$ SEM, and $n = 6$ for each condition.

Figure 4. **β3-YFP and α6-YFP expression in neuronal cells**. **A**. β3 and β2 nAChR subunits are localized similarly in N2a cells. N2a cells expressing α4β2-CFPβ3-YFP receptors were imaged live with spectral confocal microscopy. Spectral images were acquired and specific β3-YFP and β2-CFP signals were extracted with linear unmixing. Green (β3-YFP, panel i) and red (β2-CFP, panel ii) pseudocolor was assigned, and yellow (Merge, panel iii) indicates colocalized proteins. Pixel intensities for the YFP and CFP channel were plotted (panel iv) along a line (panel iii) transecting the imaged cell. **B**. β3 and α4 nAChR subunits are localized similarly in N2a cells. N2a cells expressing

α4-CFPβ2β3-YFP receptors were imaged live as in *A.* **C**. α6 and β2 nAChR subunits are localized similarly in N2a cells. N2a cells expressing α6-YFPβ2-CFP were imaged live as in *A* and *B.* **D**. α4-YFP, β3-YFP, and α6-YFP are localized intracellularly and in processes in differentiated neurons. N2a cells were differentiated for two days (see Materials and Methods for details) to induce neurite outgrowth, followed by transfection with the indicated nAChR cDNA combinations plus soluble CFP to mark cellular morphology. One day after transfection, cells were imaged live as in *A-C.* Scale bar indicates 10 μm.

Figure 5. **Localization of β3* and α6* receptors in primary neurons**. **A**. β3-YFP and α6-YFP are localized in the cell soma and in dendrites in primary hippocampal neurons. E18 rat hippocampal neurons were plated and cultured for 14 days followed by transfection with the indicated nAChR cDNAs. One day after transfection, cells were imaged live. Right panel shows a higher magnification image of the boxed area in the left panel. **B**. β3* and α6* receptors are absent from axons. Neurons were transfected with the indicated nAChR cDNAs along with CFP-tau, followed by live confocal imaging as in *A.* Scale bar indicates 10 μm.

Figure 6. **FRET reveals assembly of β3 and α6 nAChR subunits with α4 and β2**. **A**. Nicotinic receptor FRET schematic diagram. Grey cylinders indicate nAChR subunits, whereas cyan or yellow cylinders attached to nAChR subunits indicate CFP or YFP, respectively. FRET between nAChR subunits employed the acceptor photobleaching method. When subunits are assembled, 439 nm excitation of CFP (donor) results in some

emission of CFP at 485 nm, and some non-radiative transfer of energy (FRET) to YFP (acceptor) and resulting in emission at 535 nm. Acceptor photobleaching reveals FRET by measuring incremental dequenching of CFP during photodestruction of YFP with high-power 514 nm excitation. **B**. β3 assembles with β2 in the presence of α4. N2a cells expressing α4β2-CFPβ3-YFP receptors were imaged live for FRET. The 439 nm laser line was coupled to a confocal microscope equipped with spectral imaging capabilities; this instrument generated spectral images before and after photodestruction of YFP using the 514 nm laser. Specific CFP and YFP signals were generated with linear unmixing as described in Materials and Methods. YFP and CFP intensity throughout the cell before and after YFP photodestruction is shown using intensity scaling. **C**. Plot of β3-YFP and β2-CFP intensity during incremental photodestruction of β3-YFP. Normalized data from a representative cell were fitted to an exponential decay. **D**. β3 assembles with α4 in the presence of β2. N2a cells expressing α4-CFPβ2β3-YFP were imaged live for FRET as described in *B*. **E**. Plot of β3-YFP and α4-CFP intensity during incremental photodestruction of β3-YFP, similar to *C*. **F**. α6 assembles with β2. N2a cells expressing α6-YFPβ2-CFP were imaged live for FRET as described in *B*. **G**. Plot of α6-YFP and β2-CFP intensity during incremental photodestruction of α6-YFP, similar to *C*. Scale bar indicates 10 μm.

Figure 7. **β3 specifically assembles with α4β2 nAChRs**. **A**. Fluorescently labeled nicotinic receptor pentamers assayed for FRET in this experiment. N2a cells expressing the indicated receptor pentamers were assayed live for FRET using the acceptor photobleaching method. **B**. Linear plots of donor (CFP) dequenching versus acceptor

Molecular Pharmacology Fast Forward. Published on October 11, 2007 as DOI: 10.1124/mol.107.039180
This article has not been copyedited and formatted. The final version may differ from this version.

(YFP) photodestruction for nAChRs with the indicated fluorescent subunits. FRET efficiency was calculated by extrapolating linear regression plots to 100% YFP photodestruction as described in Materials and Methods. **C**. Specific FRET signal detected between β3 and α4 or β2. The FRET efficiency for the given donor-acceptor pair was calculated from the linear plot shown in *B* as described in Materials and Methods. FRET between β3-YFP and mGAT1-CFP or GluCl β-CFP was measured as a specificity control. **D**. FRET efficiency for β3-YFP does not depend on the insertion site in the M3-M4 loop. Two β3-YFP constructs, β3-YFP^{P379} and β3-YFP^{G367}, were compared for their ability to assemble with α4β2-CFP as measured by FRET. FRET efficiency was calculated as in *C*. Error bars are $\pm$ SEM and n = 5-15 cells for each condition. *** denotes $p \leq 0.001$, ** denotes $p \leq 0.01$.

Figure 8. **α6 specifically assembles with α4 and β2 nAChR subunits**. **A**. Fluorescently labeled nicotinic receptor pentamers assayed for FRET in this experiment. N2a cells expressing the indicated receptor pentamers were assayed live for FRET using the acceptor photobleaching method. **B**. Linear plots of donor (CFP) dequenching versus acceptor (YFP) photodestruction for nAChRs with the indicated fluorescent subunits. FRET efficiency was calculated by extrapolating linear regression plots to 100% YFP photodestruction as described in Materials and Methods. **C**. Specific FRET signal detected between α6 and α4 or β2. The FRET efficiency for the given donor-acceptor pair was calculated from the linear plot shown in *B* as described in Materials and Methods. FRET between α6-YFP and mGAT1-CFP or GluCl β-CFP was measured as a specificity control. **D**. FRET efficiency for α6-YFP does not depend on the insertion site

Molecular Pharmacology Fast Forward. Published on October 11, 2007 as DOI: 10.1124/mol.107.039180
This article has not been copyedited and formatted. The final version may differ from this version.

in the M3-M4 loop. Three α6-YFP constructs, α6-YFP^{A405}, α6-YFP^{G387}, and α6-YFP^{G366} were compared for their ability to assemble with β2-CFP as measured by FRET. FRET efficiency was calculated as in *C*. Error bars are ± SEM and n = 5-15 cells for each condition. *** denotes $p \leq 0.001$, ** denotes $p \leq 0.01$.

Figure 9. **FRET reveals assembly of α6β2β3 nAChRs**. **A**. Fluorescently labeled nicotinic receptor pentamers assayed for FRET in this experiment. N2a cells expressing the indicated receptor pentamers were assayed live for FRET using the acceptor photobleaching method. **B**. Linear plots of donor (CFP) dequenching versus acceptor (YFP) photodestruction for nAChRs with the indicated fluorescent subunits. FRET efficiency was calculated by extrapolating linear regression plots to 100% YFP photodestruction as described in Materials and Methods. **C**. Specific FRET signal detected between α6-YFP and β2-CFP with β3 present, α6-YFP and β3-CFP with β2 present, and β2-YFP and β3-CFP with α6 present. The FRET efficiency for the given donor-acceptor pair was calculated from the linear plot shown in *B* as described in Materials and Methods. Error bars are ± SEM and n = 10-15 cells for each condition.

Figure 10. **β3 and α6 subunit stoichiometry studied by FRET**. **A**. Fluorescently labeled nicotinic receptor pentamers assayed for FRET in this experiment. N2a cells expressing the indicated receptor pentamers were assayed live for FRET using the acceptor photobleaching method. **B**. Linear plots of donor (CFP) dequenching versus acceptor (YFP) photodestruction for nAChRs with the indicated fluorescent subunits. FRET efficiency was calculated by extrapolating linear regression plots to 100% YFP

Molecular Pharmacology Fast Forward. Published on October 11, 2007 as DOI: 10.1124/mol.107.039180
This article has not been copyedited and formatted. The final version may differ from this version.

photodestruction as described in Materials and Methods. **C**. α6-containing receptors have multiple α6 subunits whereas β3-containing receptors have only one β3 subunit. The FRET efficiency for the given donor-acceptor pair was calculated from the linear plot shown in *B* as described in Materials and Methods. **D**, **E,** and **F**. Linear plots of donor (CFP) dequenching versus acceptor (YFP) photodestruction for nAChRs with the indicated fluorescent subunits. FRET efficiency was calculated by extrapolating linear regression plots to 100% YFP photodestruction as described in Materials and Methods. **G**. β3 co-expression with α4β2 or α6β2 receptors reduces FRET between YFP and CFP-labeled α subunits. FRET *E* values for a given subunit combination was calculated from the linear plot in *D, E,* or *F*. Error bars are $\pm$ SEM and n = 10-15 cells for each condition. *** denotes $p \leq 0.001$, * denotes $p \leq 0.05$.

Figure 11. **Distinct plasma membrane localization for α4β2 versus β3* and α6* receptors**. **A**. Plasma membrane localization of α4β2 receptors. N2a cells plated on PEI, expressing α4-YFPβ2 receptors were imaged live under TIRF illumination. Arrows indicate α4β2 receptors in distal parts of membrane protrusions. Epifluorescence (non-TIRF) images and bright-field images are shown for reference. For all images, scale bar indicates 10 μm. **B**. Filopodia in N2a cells. N2a cells were plated as in *A* and stained with rhodamine-phalloidin to mark actin filaments (left panel, arrows) in the cytoplasm and in filopodia-like protrusions. Cells were imaged with confocal microscopy. Cells were treated with latrunculin B to disrupt actin filaments (right panel). **C** and **D**. Lattice-like and punctate localization of α4β2β3-YFP and α6-YFPβ2 receptors on the plasma membrane. N2a cells expressing the indicated nAChR subunits were imaged in TIRF

mode as in *A*. Epifluorescence and bright field images are shown for reference. **E**. Syntaxin1A plasma membrane localization is similar to β3 and α6 nicotinic receptors. N2a cells expressing YFP-syntaxin1A were imaged as in *A*, *C*, and *D*. **F**. β3-YFP subunits on the plasma membrane are functional. N2a cells expressing either α4-YFPβ2 or α4β2β3-YFP^{V13S} were studied using whole-cell patch clamp electrophysiology. Voltage-clamped cells were stimulated with 1 μM ACh for 500 ms. A representative response from the indicated nAChR subtype is shown. Scale bar indicates 300 pA and 500 ms. **G**. Quantification of electrophysiology data in *F*. Peak current responses from α4-YFPβ2 and α4β2β3-YFP^{V13S} (1 μM stimulation) were averaged for four cells. *** denotes $p \leq 0.001$.

Molecular Pharmacology Fast Forward. Published on October 11, 2007 as DOI: 10.1124/mol.107.039180
This article has not been copyedited and formatted. The final version may differ from this version.

Table 1. **FRET Efficiency Calculations for Nicotinic ACh Receptors with Various Subunit Compositions**. "Y" refers to YFP and "C" refers to CFP. Unless noted otherwise, all experiments with α6 and β3 subunits were performed with $\alpha6^{A405}$ and $\beta3^{P379}$. Data are reported as mean FRET *E* (%) ± SEM. *n* refers to the number of independently analyzed cells.

Subunit Composition	FRET *E* (%)	*n*
α4C/β2Y	29 ± 2	10
α4/β2C/β3Y	22 ± 2	9
α4C/β2/β3Y	20 ± 2	8
β3Y/GAT1C	-3 ± 3	9
$\alpha4/\beta2C/\beta3Y^{G367}$	22 ± 1	7
α6Y/β2C	36 ± 2	12
α6Y/GAT1C	1 ± 4	9
$\alpha6Y^{G387}/\beta2C$	38 ± 2	7
$\alpha6Y^{G366}/\beta2C$	29 ± 2	11
α6Y/β2C/β3	32 ± 2	13
α6Y/β2/β3C	25 ± 3	8
α6/β2Y/β3C	36 ± 2	14
α4Y/α4C/β2	22 ± 2	10
α4/β2Y/β2C	16 ± 2	9
α6Y/α6C/β2	28 ± 2	22
α4/β2/β3Y/β3C	3 ± 1	10

Molecular Pharmacology Fast Forward. Published on October 11, 2007 as DOI: 10.1124/mol.107.039180
This article has not been copyedited and formatted. The final version may differ from this version.

α4Y/α4C/β2/β3	14 ± 1	10
α6Y/α6C/β2/β3	21 ± 1	10
α6Y/α4C/β2	22 ± 1	21
α6Y/α4C/β2/β3	21 ± 2	11
β3Y/GluCl βC	6 ± 4	5
α6Y/GluCl βC	14 ± 2	5

Figure 1

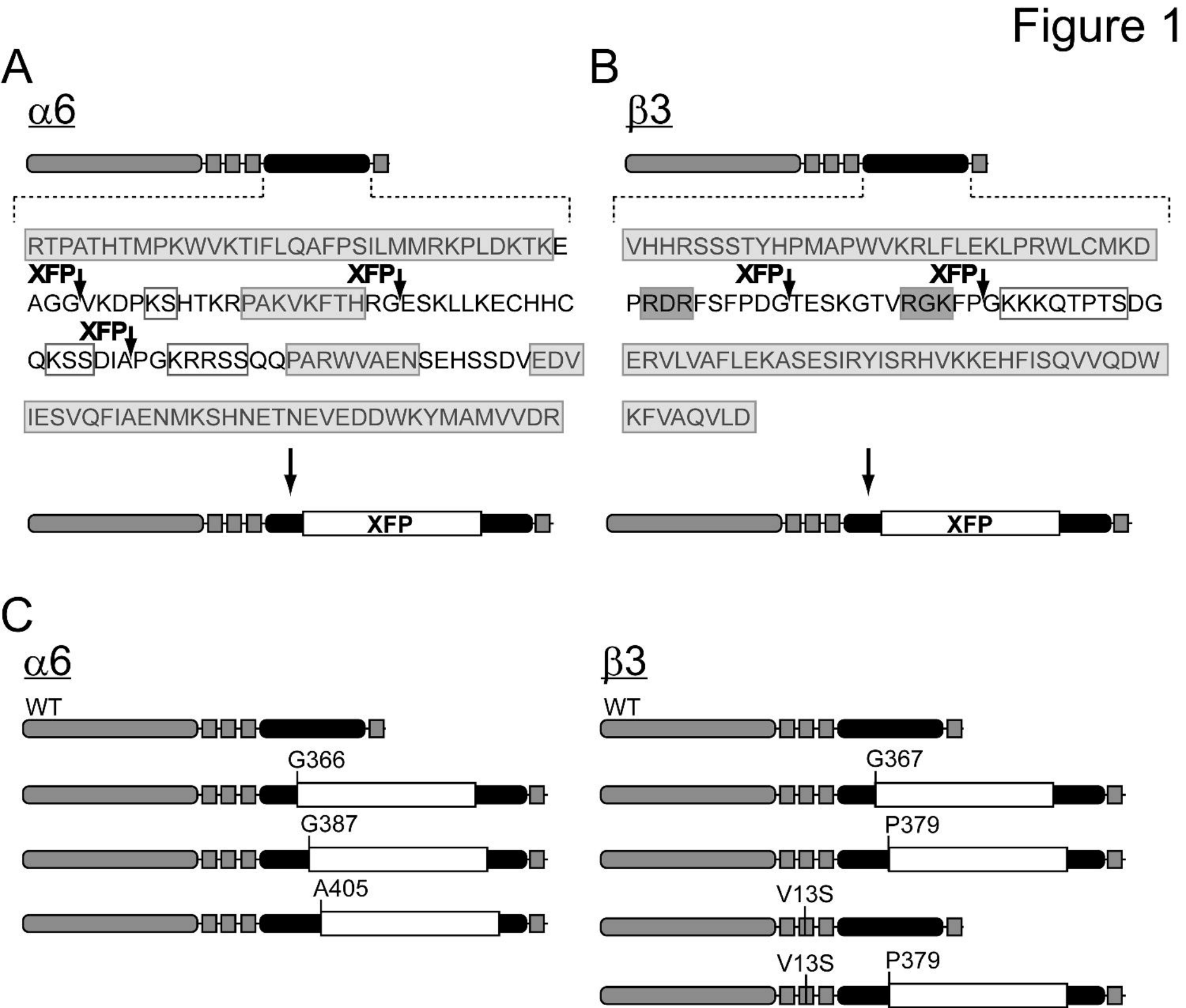
A
α6
RTPATHTMPKWVKTIFLQAFPSILMMRKPLDKTKE
XFP
XFP
AGGVKDPKSHTKRPAKVKFTHRGESKLLKECHHC
XFP
QKSSDIAPGKRRSSQQPARWVAENSEHSSDVEDV
IESVQFIAENMKSHNETNEVEDDWKYMAMVVDR
XFP
B
β3
VHHRSSSTYHPMAPWVKRLFLEKLPRWLCMKD
XFP
XFP
PRDRFSFPDGTESKGTVRGKFPGKKKQTPTSDG
ERVLVAFLEKASESIRYISRHVKKEHFISQVVQDW
KFVAQVLD
XFP
C
α6
WT
G366
G387
A405
β3
WT
G367
P379
V13S
V13S
P379

Figure 2

A

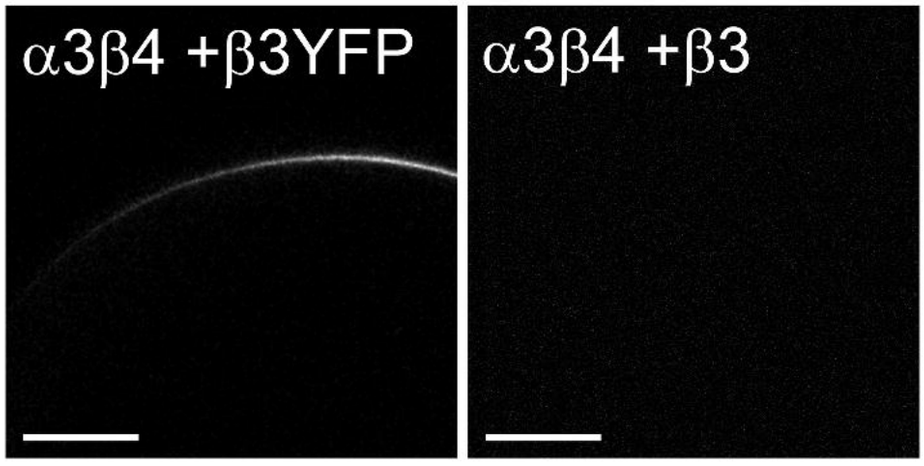
α3β4 +β3YFP
α3β4 +β3

B

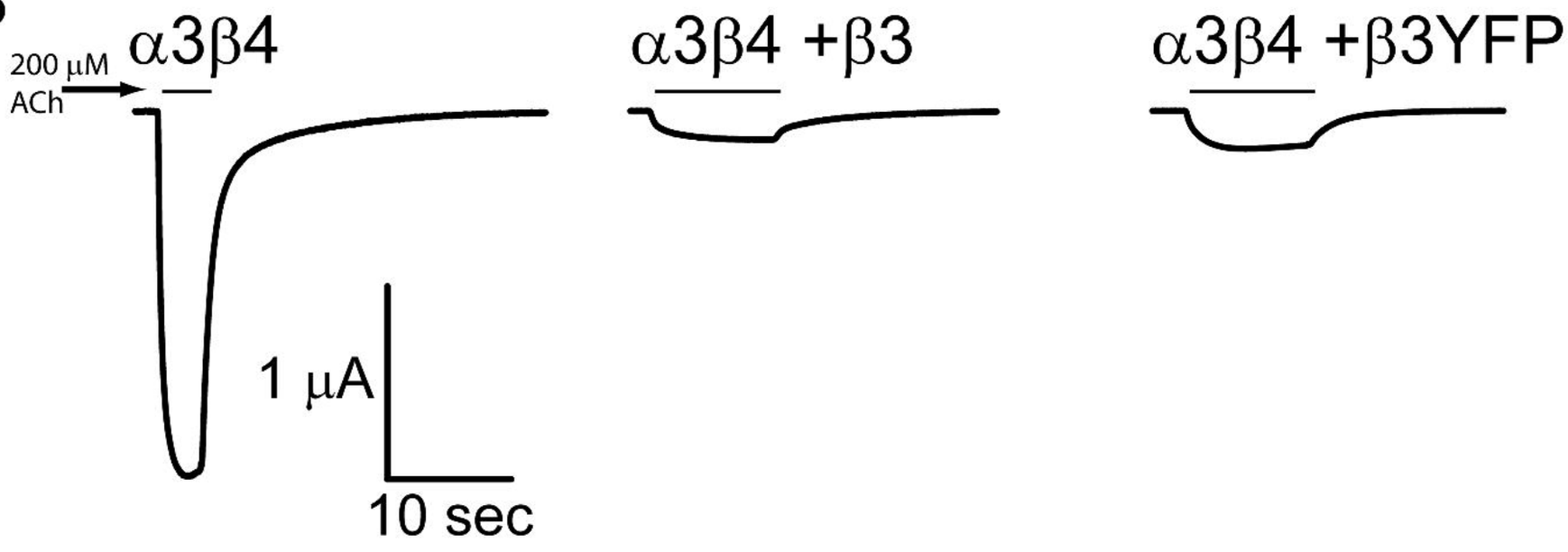
200 μM
ACh
α3β4
α3β4 +β3
α3β4 +β3YFP
1 μA
10 sec

C

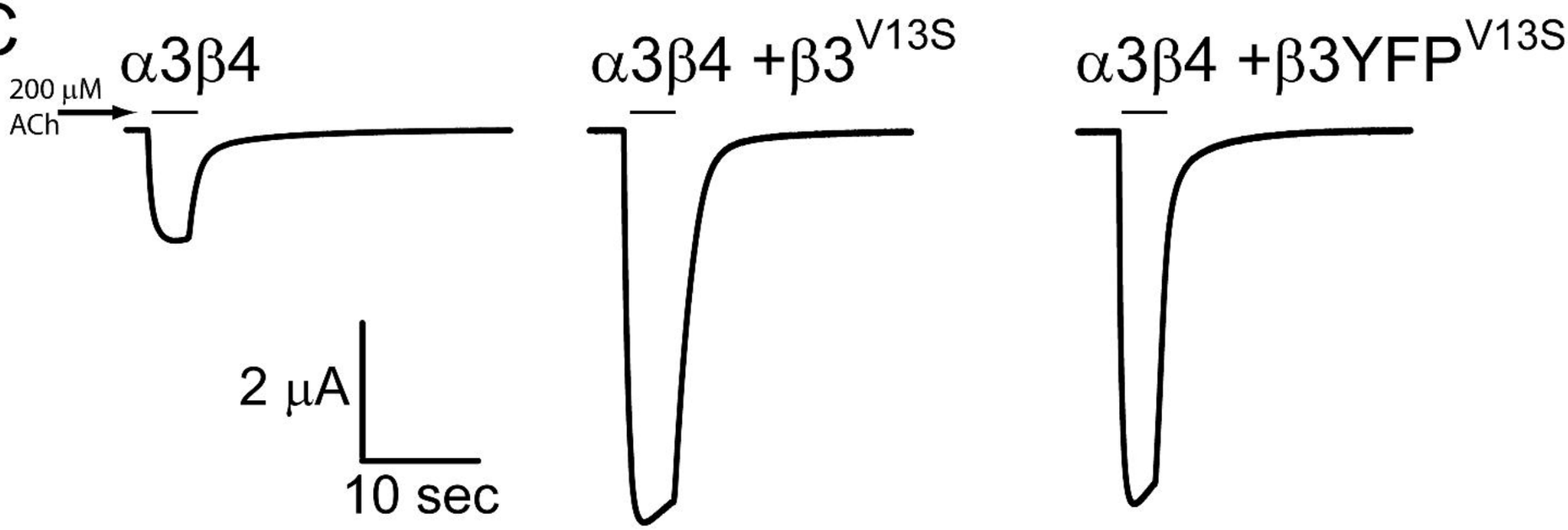
200 μM
ACh
α3β4
α3β4 +β3V13S
α3β4 +β3YFPV13S
2 μA
10 sec

Figure 3

A

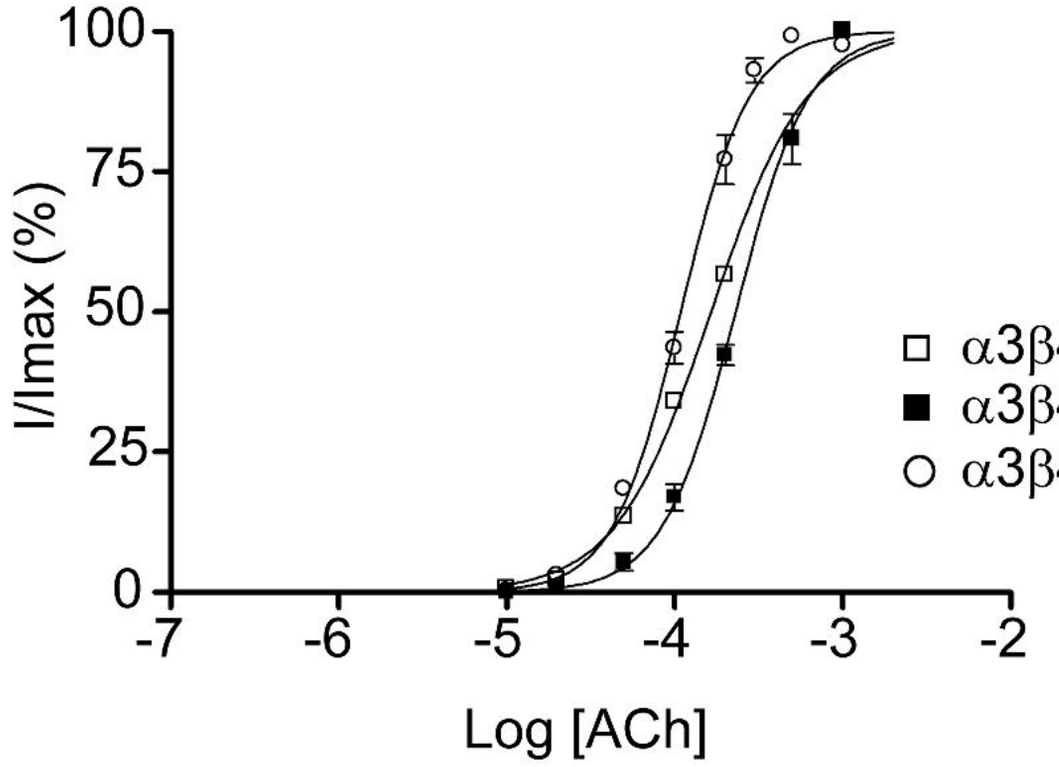

	EC_{50} (μM)	n (Hill)
□ α3β4	165 ± 9	1.5 ± 0.1
■ α3β4 +β3	230 ± 22	2.0 ± 0.3
○ α3β4 +β3YFP	109 ± 8	2.1 ± 0.3

B

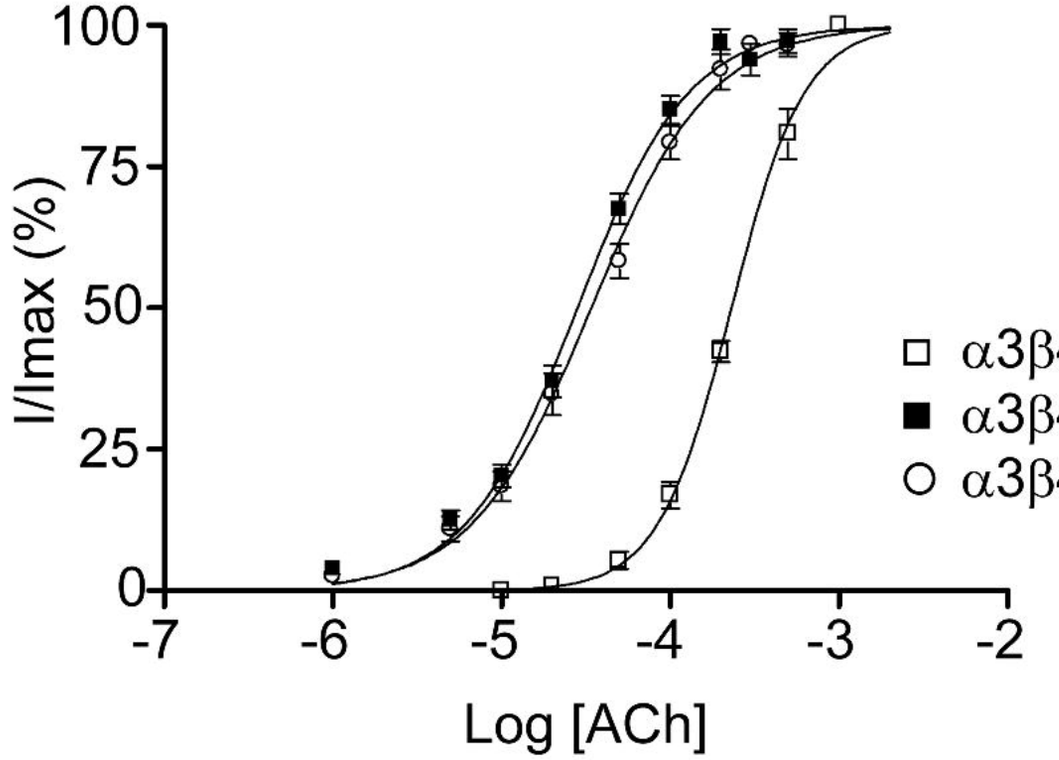

	EC_{50} (μM)	n (Hill)
□ α3β4 +β3	230 ± 22	2.0 ± 0.3
■ α3β4 +$β3^{V13S}$	28 ± 3	1.3 ± 0.2
○ α3β4 +$β3YFP^{V13S}$	34 ± 3	1.2 ± 0.1

Figure 4

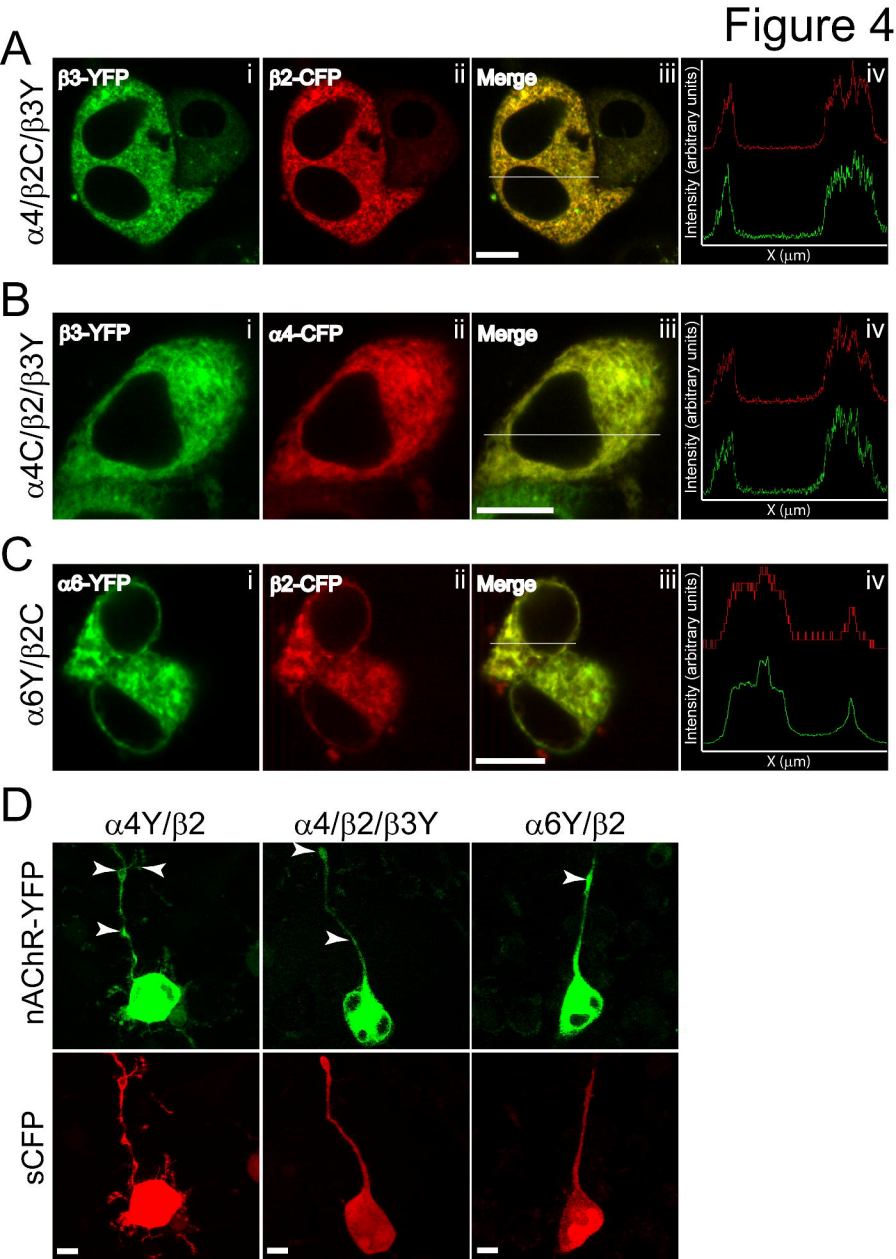
A
α4/β2C/β3Y
β3-YFP
i
β2-CFP
ii
Merge
iii
iv
Intensity (arbitrary units)
X (μm)
B
α4C/β2/β3Y
β3-YFP
i
α4-CFP
ii
Merge
iii
iv
Intensity (arbitrary units)
X (μm)
C
α6Y/β2C
α6-YFP
i
β2-CFP
ii
Merge
iii
iv
Intensity (arbitrary units)
X (μm)
D
α4Y/β2
α4/β2/β3Y
α6Y/β2
nAChR-YFP
sCFP

Figure 5

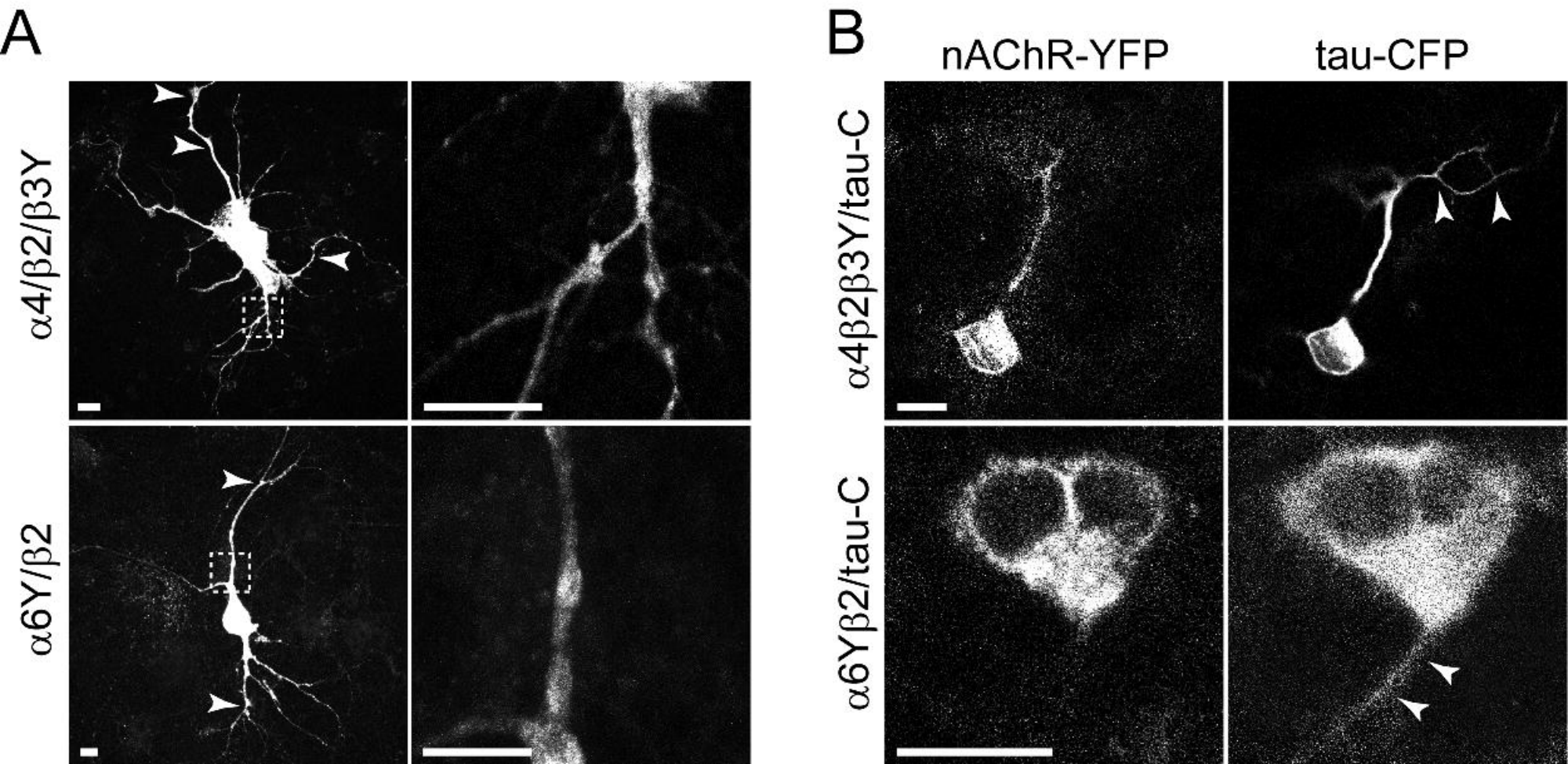

Figure 6

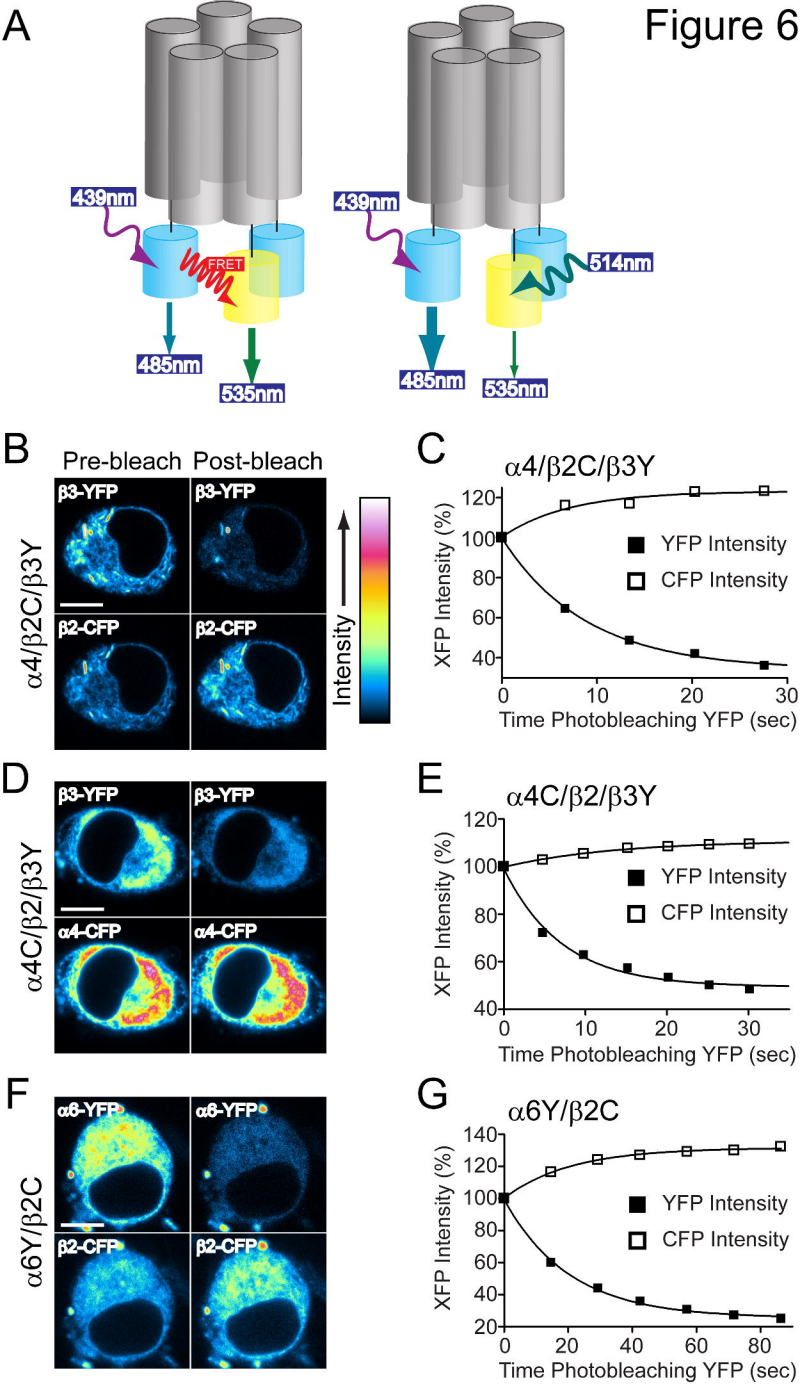
A
439nm
FRET
485nm
535nm
439nm
514nm
485nm
535nm
B
Pre-bleach
Post-bleach
β3-YFP
β3-YFP
β2-CFP
β2-CFP
α4/β2C/β3Y
Intensity
C
α4/β2C/β3Y
XFP Intensity (%)
YFP Intensity
CFP Intensity
Time Photobleaching YFP (sec)
D
β3-YFP
β3-YFP
α4-CFP
α4-CFP
α4C/β2/β3Y
E
α4C/β2/β3Y
XFP Intensity (%)
YFP Intensity
CFP Intensity
Time Photobleaching YFP (sec)
F
α6-YFP
α6-YFP
β2-CFP
β2-CFP
α6Y/β2C
G
α6Y/β2C
XFP Intensity (%)
YFP Intensity
CFP Intensity
Time Photobleaching YFP (sec)

Figure 7

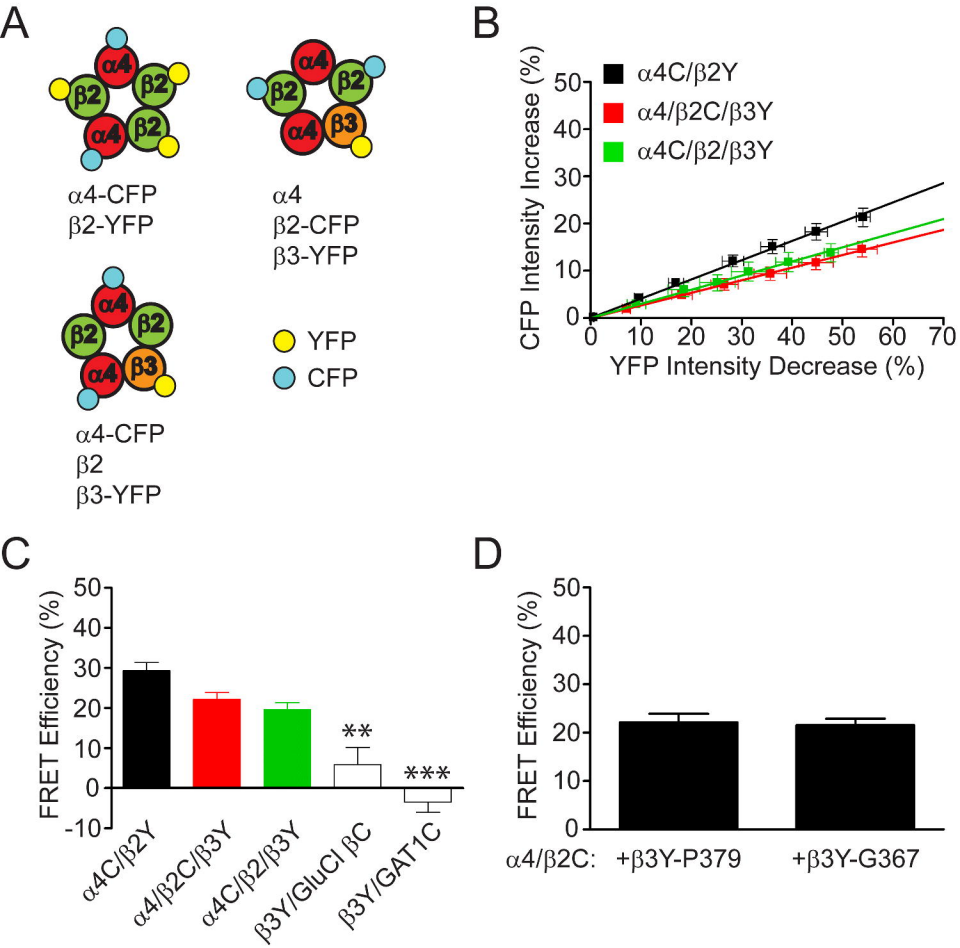
A
α4
β2
β3
α4-CFP
β2-YFP
α4
β2-CFP
β3-YFP
α4-CFP
β2
β3-YFP
YFP
CFP
B
α4C/β2Y
α4/β2C/β3Y
α4C/β2/β3Y
CFP Intensity Increase (%)
YFP Intensity Decrease (%)
C
FRET Efficiency (%)
**
***
α4C/β2Y
α4/β2C/β3Y
α4C/β2/β3Y
β3Y/GluCl βC
β3Y/GAT1C
D
FRET Efficiency (%)
α4/β2C: +β3Y-P379
+β3Y-G367

Figure 8

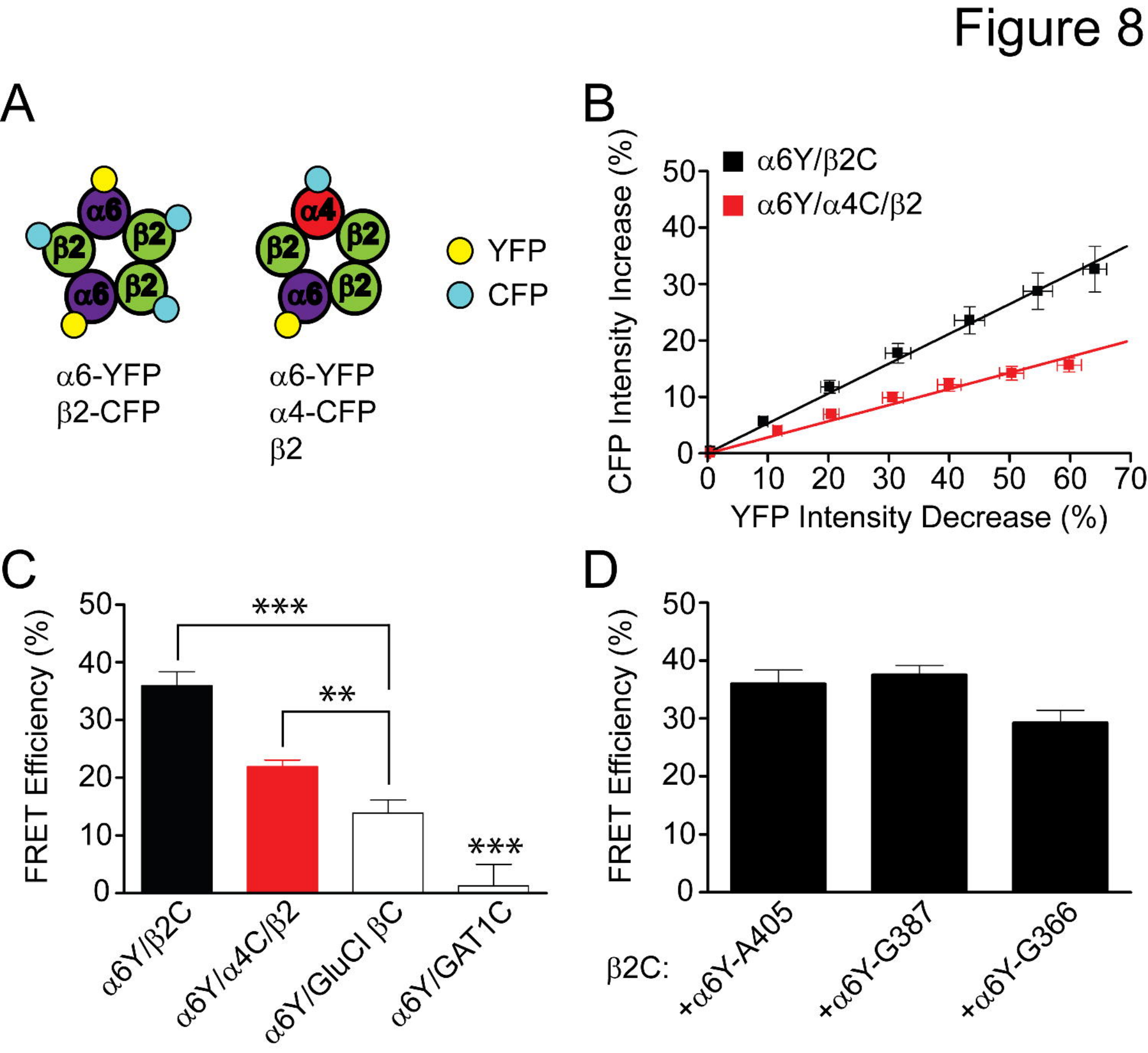
A
α6
β2
β2
α6
β2
α4
β2
β2
α6
β2
YFP
CFP
α6-YFP
β2-CFP
α6-YFP
α4-CFP
β2
B
α6Y/β2C
α6Y/α4C/β2
CFP Intensity Increase (%)
YFP Intensity Decrease (%)
0
10
20
30
40
50
60
70
C
FRET Efficiency (%)
***
**
***
α6Y/β2C
α6Y/α4C/β2
α6Y/GluCl βC
α6Y/GAT1C
D
FRET Efficiency (%)
β2C:
+α6Y-A405
+α6Y-G387
+α6Y-G366

Figure 9

A

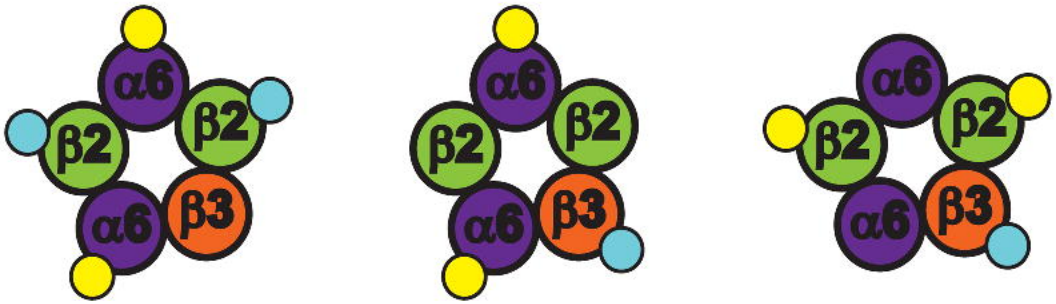

α6-YFP
β2-CFP
β3

α6-YFP
β2
β3-CFP

α6
β2-YFP
β3-CFP

B

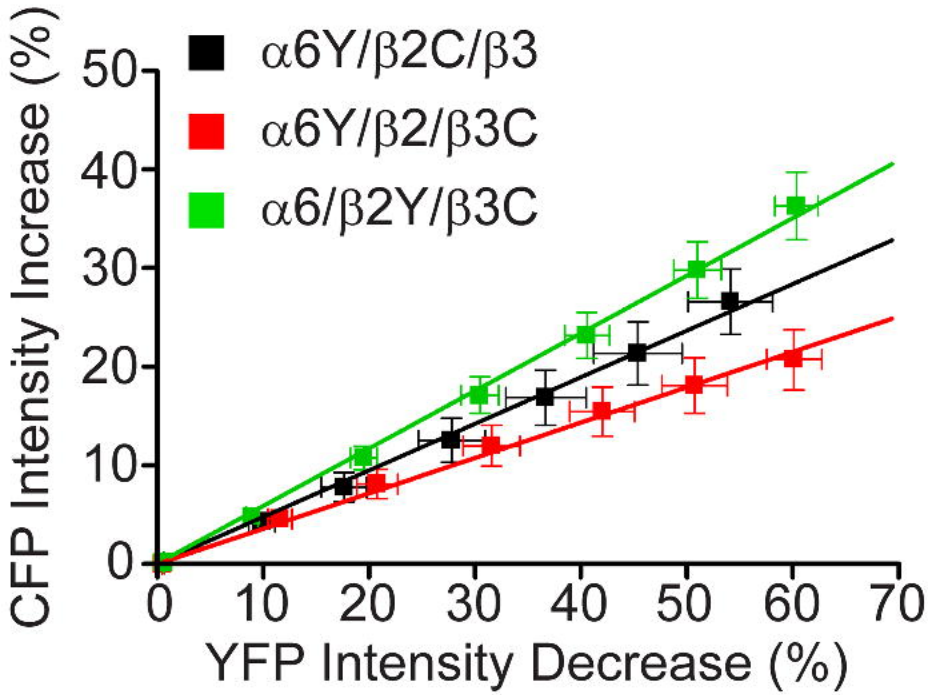

C

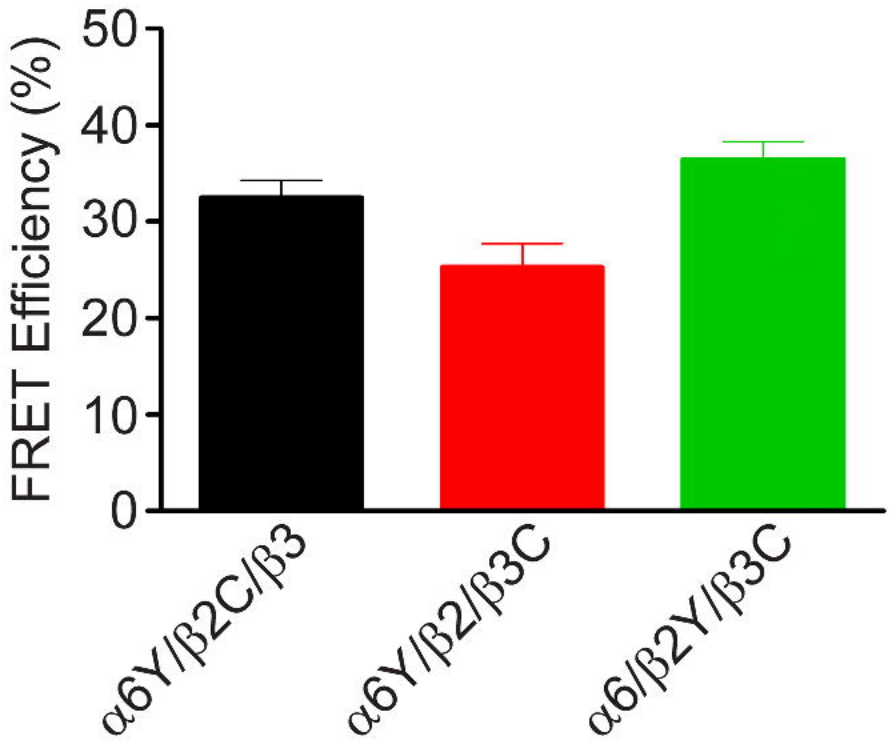

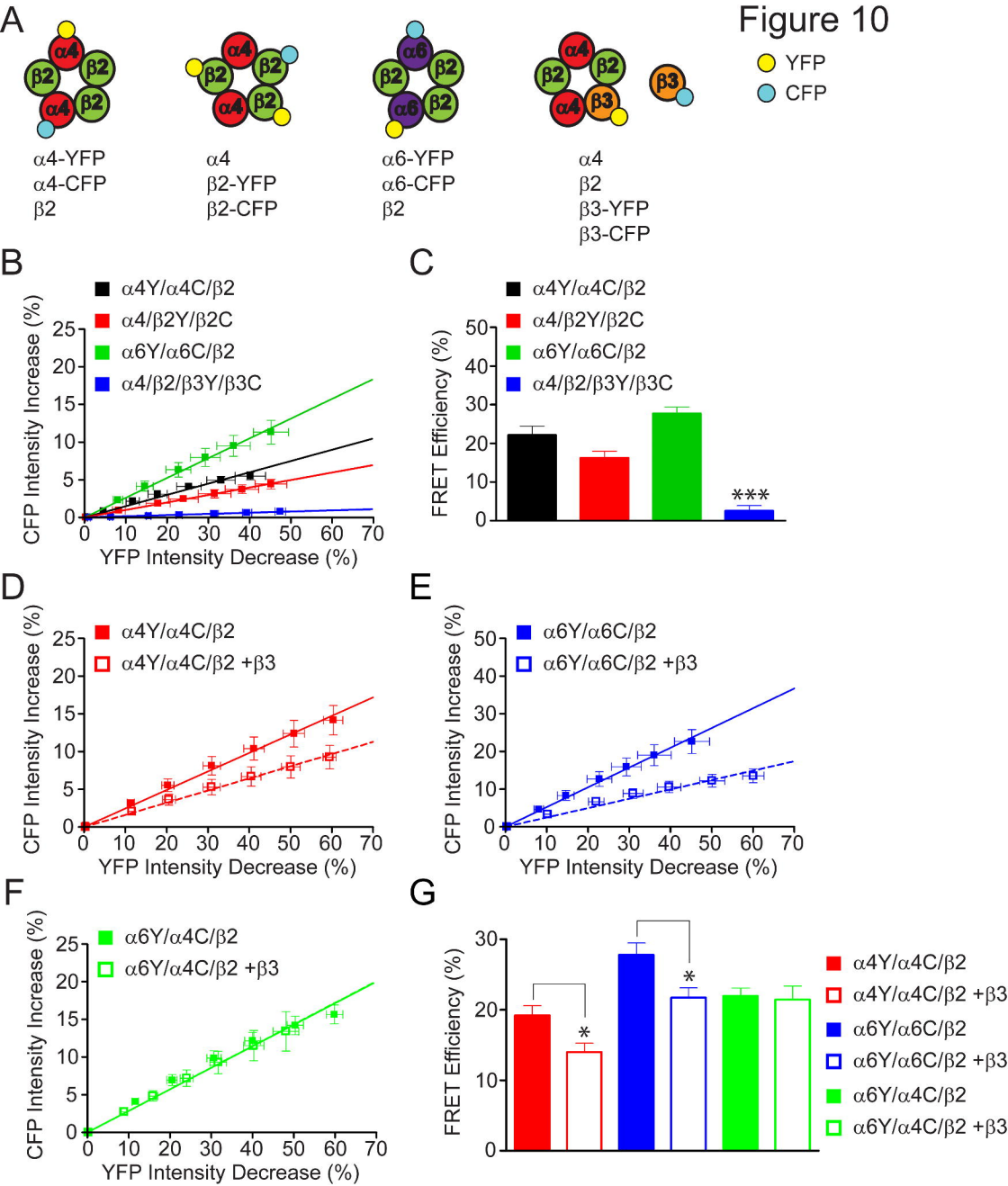
Figure 10
YFP
CFP
A
α4
β2
α6
β3
α4-YFP
α4-CFP
β2
α4
β2-YFP
β2-CFP
α6-YFP
α6-CFP
β2
α4
β2
β3-YFP
β3-CFP
B
α4Y/α4C/β2
α4/β2Y/β2C
α6Y/α6C/β2
α4/β2/β3Y/β3C
CFP Intensity Increase (%)
YFP Intensity Decrease (%)
C
FRET Efficiency (%)
***
D
α4Y/α4C/β2
α4Y/α4C/β2 +β3
CFP Intensity Increase (%)
YFP Intensity Decrease (%)
E
α6Y/α6C/β2
α6Y/α6C/β2 +β3
CFP Intensity Increase (%)
YFP Intensity Decrease (%)
F
α6Y/α4C/β2
α6Y/α4C/β2 +β3
CFP Intensity Increase (%)
YFP Intensity Decrease (%)
G
FRET Efficiency (%)
*
*
α4Y/α4C/β2
α4Y/α4C/β2 +β3
α6Y/α6C/β2
α6Y/α6C/β2 +β3
α6Y/α4C/β2
α6Y/α4C/β2 +β3

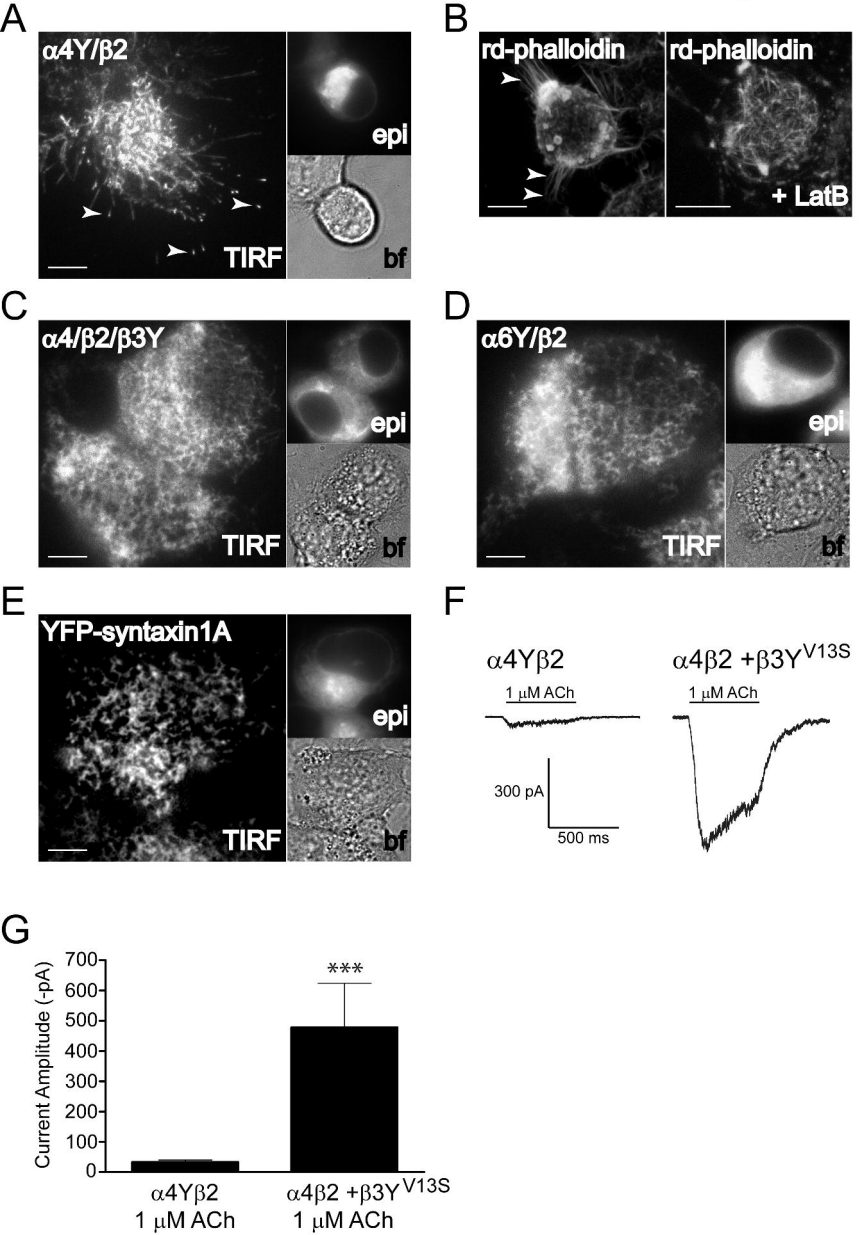
A
α4Y/β2
epi
TIRF
bf
B
rd-phalloidin
rd-phalloidin
+ LatB
C
α4/β2/β3Y
epi
TIRF
bf
D
α6Y/β2
epi
TIRF
bf
E
YFP-syntaxin1A
epi
TIRF
bf
F
α4Yβ2
1 μM ACh
300 pA
500 ms
α4β2 +β3Y V13S
1 μM ACh
G
Current Amplitude (-pA)
700
600
500
400
300
200
100
0
***
α4Yβ2
1 μM ACh
α4β2 +β3Y V13S
1 μM ACh

Supplemental Data

Table 1. **nAChRs containing α6 subunits assayed for functional activity**. No significant nAChR function was detected in cells expressing the following subunit combinations. The identity of the injected/transfected subunits, the expression/assay system, and reference (if applicable) using the specific α6 expression plasmid is listed. Unless indicated otherwise, mouse subunits were used. For non-mouse subunits, the following notation indicates the species: ^{H} – human, ^{R} – rat, ^{C} – chick. In some cases, "sensitizing", hypersensitive mutations ($\alpha6^{L9'S}$ or $\beta3^{V13'S}$) in α6 or β3 were used. Abbreviations: TEVC – two electrode voltage clamp; HEK – human embryonic kidney 293 cells; WCP – whole cell patch clamp; N2a – mouse N2a neuroblastoma cells; Fura – Fura-2 Ca^{++} flux assay.

Subunits expressed	Expression/Assay system	Reference
α6β2	*Xenopus* oocyte - TEVC	this study
α6β2β3	*Xenopus* oocyte – TEVC	this study
$\alpha6^{L9'S}\beta2$	*Xenopus* oocyte – TEVC	this study
$\alpha6^{L9'S}\beta2\beta3$	*Xenopus* oocyte – TEVC	this study
$\alpha4\alpha6^{L9'S}\beta2$	*Xenopus* oocyte – TEVC	this study
α6β4	*Xenopus* oocyte – TEVC	this study
α6β4β3	*Xenopus* oocyte – TEVC	this study
$\alpha6^{H}\beta2$	*Xenopus* oocyte – TEVC	(1)
$\alpha6^{R}\beta2$	*Xenopus* oocyte – TEVC	N/A
$\alpha6^{C}\beta2$	*Xenopus* oocyte – TEVC	(1)

$\alpha3\alpha6^{L9'S}\beta4$	*Xenopus* oocyte – TEVC	this study
$\alpha6\beta3^{V13'S}\beta4$	*Xenopus* oocyte – TEVC	this study
α6-YFPβ2	*Xenopus* oocyte – TEVC	this study
α6-YFPβ4	*Xenopus* oocyte – TEVC	this study
α6β2 +Ric-3	*Xenopus* oocyte – TEVC	this study
α6-YFPβ2	N2a – Fura, WCP	this study
α6-YFPβ2β3	N2a – Fura, WCP	this study
α6-YFPβ4	N2a – WCP	this study
α6β2	HEK – Fura, WCP	this study
α6-YFPβ2	HEK – Fura, WCP	this study

References

1. Kuryatov, A., Olale, F., Cooper, J., Choi, C., and Lindstrom, J. (2000) *Neuropharmacology* **39**(13), 2570-2590